This manuscript has been submitted for publication in *JGR: Solid Earth*. Please note that this article has not been peer-reviewed before and is currently undergoing peer review for the first time. Subsequent versions of this manuscript may have slightly different content.

Effects of Stress and Friction Heterogeneity on Spatiotemporal Complexity of Seismic and Aseismic Slip on Strike-Slip Faults

Jeena Yun[1], Alice-Agnes Gabriel[1,2], Dave A. May[1], and Yuri Fialko[1]

[1]Scripps Institution of Oceanography, University of California San Diego, La Jolla, CA, USA
[2]Department of Earth and Environmental Sciences, Ludwig-Maximilians Universität München, Munich, Germany

Key Points:

- Variable hypocenter depths in 2D models of strike-slip faults require heterogeneity in rate-and-state friction parameter $(a - b)$.
- Slip complexity generally increases with the ratio of seismogenic zone width to nucleation size, but this correlation is model-dependent.
- Models using slip law produce fewer partial ruptures, smaller stress drops, and lower peak slip rates compared to models using aging law.

Corresponding author: Jeena Yun, `j4yun@ucsd.edu`

Abstract
Numerical and laboratory models of earthquake cycles on faults governed by rate-and-state friction often show cycle-invariant behavior, while natural faults exhibit considerable variability in slip history. Possible explanations include heterogeneities in fault stress and frictional properties. We investigate how various types of heterogeneity in simulations of quasi-dynamic sequences of seismic and aseismic slip affect rupture complexity, hypocenter location, and slow slip events (SSEs). We model a 2D vertical strike-slip fault and study the roles of self-affine fractal heterogeneities in normal stress, rate-and-state parameter $(a - b)$, and characteristic slip-weakening distance, as well as the effects of a low-rigidity fault zone. We find that only a combination of heterogeneous parameters introduces variability in the modeled rupture extent, hypocenter depth, and recurrence interval. In particular, variable hypocenter depths require velocity-strengthening patches within the velocity-weakening seismogenic zone. A low-rigidity fault zone can encourage pulse-like ruptures but adds little to slip complexity. Slip law simulations produce fewer partial ruptures, smaller stress drops, and lower peak slip rates compared to aging law simulations. We show that the ratio of the seismogenic zone thickness to nucleation size does not entirely predict slip complexity. The most complex aging law model, combining multiple heterogeneities, features system-size earthquakes preceded by cascades of partial ruptures and spontaneous SSEs. For such models, a transition from aperiodic to quasi-regular regimes requires more cycles than is typically needed to erase the effect of initial conditions. These results highlight the importance of heterogeneity in reproducing natural fault slip complexity in numerical models of earthquake sequences.

Plain Language Summary

Natural earthquakes exhibit considerable variability in their size, time, and location. In contrast, computer simulations of earthquake cycles often show cycle-invariant behavior with constant recurrence intervals and characteristic slip distributions. Possible model ingredients needed to reproduce the variable slip histories observed in nature include heterogeneities in fault properties. We investigate how various types of heterogeneity in simulations of sequences of earthquakes affect rupture complexity. We find that only a combination of multiple heterogeneities introduces variability in the modeled earthquake size, location, and recurrence interval. In particular, variable hypocenter depths require areas of stable creep within the seismogenic zone. Including a layer of less stiff material near the fault adds little to slip complexity. The most complex model in this study, combining multiple heterogeneities, features non-repeating cycles of large earthquakes preceded by a cascade of smaller foreshocks. However, the complexity transitions to periodic cycles after ~ 1700 years of simulation time, suggesting heterogeneity-induced variability in modeled slip history may only be transient. Our results also suggest that 3D effects may be important for producing and maintaining spatiotemporal complexity in fault slip.

1 Introduction

The theory of rate-and-state friction (RSF; Dieterich, 1979; Ruina, 1983) is widely used to model seismic and aseismic slip on geological faults (e.g., Barbot et al., 2012; Erickson et al., 2020; Jiang & Lapusta, 2016; Tse & Rice, 1986). Simulations of earthquake sequences on faults obeying RSF successfully reproduce many aspects of the observed behavior of natural faults, including stick-slip (e.g., V. C. Li & Rice, 1987; Lapusta et al., 2000), afterslip (Barbot et al., 2009; Helmstetter & Shaw, 2009; Perfettini & Avouac, 2007; K. Wang & Fialko, 2014), interseismic creep (Kaneko et al., 2013; Lindsey & Fialko, 2016), the Gutenberg-Richer and Omori laws (Beall et al., 2022; Cattania, 2019; Dieterich, 1994; Ito & Kaneko, 2023), and earthquake triggering (Luo & Liu, 2019; Perfettini et al., 2003a, 2003b; Wei et al., 2018).

However, a typical feature of earthquake simulators and models of sequences of earthquakes and seismic slip (SEAS) on faults governed by RSF is cycle invariance, whereby the recurrence intervals and slip patterns become constant following some initial 'spin-up' phase in which the effects of initial conditions are erased (e.g., Erickson et al., 2020; Rice, 1993; Tse & Rice, 1986; S. Wang, 2024). Such models also exhibit a limited range of earthquake nucleation depths (e.g., Barbot, 2019; Cattania, 2019; Erickson et al., 2023; Lapusta & Rice, 2003). This is in contrast to the observed seismicity patterns on natural faults that are characterized by highly irregular recurrence intervals and a wide distribution of hypocenter locations throughout the seismogenic zone (e.g., Jin & Fialko, 2020; Ross et al., 2020; Waldhauser & Schaff, 2008).

Previous studies attempted to reproduce the observed complex slip behavior by introducing inherent discreteness, e.g., by using numerical grids that are coarser than the characteristic nucleation size (e.g., Ben-Zion & Rice, 1995; Rice, 1993; Rice & Ben-Zion, 1996; Ziv & Cochard, 2006), or modifying constitutive parameters to facilitate nucleation (e.g., Cochard & Madariaga, 1996; Shaw & Rice, 2000). In continuum models, spatiotemporal complexity of slip can arise from various heterogeneities, including spatially variable frictional properties (Hillers et al., 2007; Jiang & Fialko, 2016; M. Li et al., 2025; Luo & Ampuero, 2018; Molina-Ormazabal et al., 2023), elastic moduli (Y. Huang et al., 2014; Idini & Ampuero, 2020; Thakur et al., 2020), and fault geometry (Cattania & Segall, 2021; Ozawa & Ando, 2021; Tal & Gabrieli, 2024; Yin et al., 2023).

Alternatively, it was shown that increases in slip complexity can result from decreases in the critical length scale of the nucleation process relative to the characteristic fault size (Cattania, 2019; Erickson et al., 2011; Herrendörfer et al., 2015; Y. Liu & Rice, 2007; Nie & Barbot, 2022). Numerical models show less regular cycles of earthquakes for smaller characteristic nucleation size, with the emergence of partial ruptures (e.g., Barbot, 2019; Cattania & Segall, 2019; Lapusta et al., 2000) and realistic earthquake statistics such as the Omori-type aftershock decay or the frequency-magnitude relation (e.g., Cattania, 2019). However, the respective models still exhibit a narrow range of hypocenter locations, mostly limited to the edges of the seismogenic zone (e.g., Barbot, 2019; Lapusta & Rice, 2003).

In addition, the largely empirical RSF framework involves a choice of the functional form of the so-called evolution law for the state variable (e.g., Ampuero & Rubin, 2008; Dieterich, 1979; Ruina, 1983). The two most common choices are the aging law (Dieterich, 1979) and the slip law (Ruina, 1983), but other forms of the evolution law were proposed as well (e.g., Kato & Tullis, 2001; Linker & Dieterich, 1992; Nagata et al., 2012; Yoshida et al., 2020). Different formulations are meant to explain different aspects of available experimental data. For example, the aging law well captures the time-dependent healing of the rock surface in slide-hold-slide and stick-slip experiments (e.g., Beeler et al., 1994; Dieterich & Kilgore, 1994; Mitchell et al., 2015, 2016), while the slip law seemingly better accounts for the evolution of friction in velocity stepping experiments with large velocity changes (Ampuero & Rubin, 2008; Bayart et al., 2006; Pignalberi et al., 2024). These empirical laws have different intrinsic length scales and predict different slip evolutions away from the steady state (Ampuero & Rubin, 2008). How various choices of the state evolution law may affect complexity of the system behavior and a fault response to external stress perturbations is not well understood.

In this study, we investigate the effects of various types of heterogeneity on rupture complexity, hypocenter location, and aseismic transients in simulated earthquake and aseismic slip sequences. Seismic cycle simulations empowered by high-performance computing enable more realistic parameterization, extensive parameter space exploration, and volume-discretized methods, addressing key knowledge gaps despite high computational costs (e.g., Taufiqurrahman et al., 2023; Uphoff et al., 2023; Erickson & Dunham, 2014; D. Liu et al., 2020; Pranger, 2020; Thakur et al., 2020). We perform a suite of quasi-dynamic seismic cycle simulations on a 2D vertical strike-slip fault in the presence of different heterogeneities on and off the fault (Sections 3.1 & 3.2), using two different state variable evolution laws (Sections 3.3 & 3.4). We document key features of the most complex models obtained in this study, including cascades of ruptures, emergence of spontaneous slow slip events, and quasi-chaotic earthquake sequences (Section 3.3). We find that heterogeneity in any single parameter is insufficient to produce sustainable complexity in a 2D quasi-dynamic framework and that the ratio of the seismogenic fault width to the characteristic nucleation length scale is not a universal predictive metric for the system complexity. Diversity in hypocenter depths is strongly affected by the presence of velocity-strengthening patches within the seismogenic zone, and less so by a low-rigidity fault zone. These results provide insights into how the system behavior, including the rupture characteristics, depends on various heterogeneities in material properties and field variables, as well as different assumed evolution laws. In a companion paper, we use the complex multi-cycle simulations developed here, incorporating heterogeneous material properties, to investigate the triggering potential of rate-and-state faults perturbed by static and dynamic stress changes from nearby earthquakes (Yun et al., 2025).

2 Methods

2.1 Models of Earthquake Sequences on Faults governed by RSF

We use the open-source code *Tandem* (Uphoff et al., 2023) to perform quasi-dynamic simulations of seismic cycles on a 2D vertical strike-slip fault (Fig. 1a). *Tandem* is based on a symmetric interior penalty discontinuous Galerkin method and is optimized for high-performance computing. *Tandem* uses the regularized version of the rate-and-state friction formulation (Lapusta et al., 2000),

$$F(\|\boldsymbol{V}\|,\theta) = a\sinh^{-1}\left[\frac{\|\boldsymbol{V}\|}{2V_0}\exp\left(\frac{f_0 + b\ln\left(V_0\theta/D_{RS}\right)}{a}\right)\right], \tag{1}$$

where F is the instantaneous friction coefficient, $\|\boldsymbol{V}\|$ is the Euclidean norm of the slip rate vector $\boldsymbol{V}$, θ is the state variable, a, b are the rate-and-state parameters for direct and evolution effect, respectively, D_{RS} is the characteristic state evolution distance, V_0 is the reference slip rate, and f_0 is the reference friction coefficient. All seismic cycle model parameters used in this study are summarized in Table 1.

The sign of $(a-b)$ determines the stability of the system. An increase in sliding velocity leads to a drop of static friction when $a - b < 0$, promoting instability, which is referred to as velocity-weakening (VW) behavior. Conversely, static friction increases when $a-b > 0$, suppressing instability, which is defined as velocity-strengthening (VS) behavior. In this study, we include shallow and deep VS regions surrounding a central VW zone, representing a 10-km-wide seismogenic zone (Fig. 1a). The rate-and-state fault is loaded from the bottom creeping zone and the far boundary with a constant velocity (V_{pl}) of 10^{-9} m/s $\approx$ 30 mm/yr corresponding to the long-term fault slip rate.

In quasi-dynamic simulations, the inertial effect is approximated by a radiation damping term $\eta\boldsymbol{V}$ (Rice, 1993):

$$-\boldsymbol{\tau} = \sigma_n F(\|\boldsymbol{V}\|,\theta)\frac{\boldsymbol{V}}{\|\boldsymbol{V}\|} + \eta\boldsymbol{V}, \tag{2}$$

where $\eta = \mu/2c_s$ is half of the shear-wave impedance with shear modulus μ and shear-wave speed c_s, and $\boldsymbol{\tau}$ and σ_n are shear and normal stresses on the fault, respectively. Although quasi-dynamic models do not capture all details of full elastodynamic solutions, they produce qualitatively comparable slip patterns at considerably lower computational cost (Kroll et al., 2023; Lapusta & Rice, 2003; Rice & Ben-Zion, 1996; Thomas et al., 2014).

The evolution of the state variable θ is governed by an ordinary differential equation. We explore the two most common end-members, the aging law (Dieterich, 1979),

$$\frac{d\theta}{dt} = 1 - \frac{\|\boldsymbol{V}\|\theta}{D_{RS}}, \tag{3}$$

and the slip law (Ruina, 1983):

$$\frac{d\theta}{dt} = -\frac{\|\boldsymbol{V}\|\theta}{D_{RS}} \ln\left(\frac{\|\boldsymbol{V}\|\theta}{D_{RS}}\right). \tag{4}$$

The ratio of the length of the seismogenic fault (W; Table 1) to the critical nucleation size is known to affect the complexity of the earthquake sequence. For 2D anti-plane simulations using the aging law (with $0.5 < a/b < 1$), the critical nucleation size (L_∞) can be expressed as follows (Rubin & Ampuero, 2005):

$$L_\infty = \frac{2}{\pi} \frac{\mu b D_{RS}}{\sigma_n (b-a)^2}. \tag{5}$$

There is no equivalent analytical form of the critical nucleation size for the slip law, as the nucleation zone continuously shrinks under slip law formulation (Ampuero & Rubin, 2008). Thus, we only compare the W/L_∞ ratios among aging law models. The critical nucleation size also controls the grid size, as the former needs to be resolved by the model. A detailed description of different model resolution requirements for each evolution law is provided in Supplementary Section S1.

We use adaptive time stepping handled by the software PETSc (Abhyankar et al., 2014; Balay et al., 1997, 2019) with a fourth-order embedded fifth-order Dormand-Prince scheme Runge-Kutta method.

2.2 Fractal Heterogeneities

We introduce band-limited self-affine fractal variations to the initial effective normal stress (σ_n^0), rate-and-state parameters ($a - b$), and the characteristic state evolution distance (D_{RS}). The self-affine fractal variation emulates a power-law distribution of many attributes of natural faults, such as the fault roughness (Lee & Bruhn, 1996; Maurer, 2024; Renard et al., 2006). Here, we approximate the effects of fault roughness by imposing fractal variations in fault-normal stress. We also impose fractal variations in RSF parameters. The 1D fractal distributions are characterized by the power spectral density $P(k)$ as follows (Andrews & Barall, 2011; Dunham et al., 2011):

$$P(k) \propto k^{-(2H+1)} \tag{6}$$

with the wavenumber k and the Hurst exponent H. The Hurst exponent $H = 1$ results in a self-similar fractal distribution, while $0 \leq H < 1$ produces a self-affine distribution. For natural faults, H is typically assumed to vary between 0.4 to 0.8 (Renard & Candela, 2017). We set $H = 0.7$ for all fractal profiles used in this study (Cattania & Segall, 2021). The fractal variation is limited between a minimum (λ_{min}) and maximum (λ_{max}) wavelengths. We explore a wide range of λ_{min} from 30 m (comparable to the critical nucleation size) to 750 m and λ_{max} from 2.5 km to 10 km (comparable to W) to identify values of λ_{min} and λ_{max} that produce most diversity in both rupture sizes (e.g., occurrence of both partial ruptures and system-size events) and hypocenter depths (i.e., widely distributed nucleation locations within the seismogenic zone).

We use a Fourier transform method (Andrews & Barall, 2011; Shi & Day, 2013) to generate the fractal profile and take an amplitude-to-wavelength ratio of 10^{-2} to scale the root-mean-square amplitude of the profile (Dunham et al., 2011). All fractal variations are tapered outside the seismogenic zone by scaling their amplitude by the distance from the nearest VW region. The fractal amplitudes are then converted into variations of parameters by applying scaling factors that match the order of magnitude of each parameter. For example, the fractal effective normal stress profile is obtained by scaling the fractal amplitude by $(\rho_c - \rho_w)g$, where $\rho_c = 2670$ kg/m^3 is density of crust, $\rho_w = 1000$ kg/m^3 is density of water, and $g = 9.8$ m/s^2 is the acceleration due to gravity. Since the fractal heterogeneity has a mean of zero, the average value for each parameter (i.e., $\overline{\sigma_n^0}$, $\overline{a-b}$, and $\overline{D_{RS}}$) remains the same for both fractal (red solid lines in Figs. 1b-d) and non-fractal (grey dashed lines in Figs. 1b-d) distributions.

2.3 Event Detection and Classification

We implement an automated event detection and classification algorithm to systematically compare the event time and hypocenter locations across different models. A seismic event is identified when the peak slip rate along the fault exceeds a threshold of 0.2 m/s for more than 0.5 s at more than one of the evaluation points which are spaced every 200 m along the fault. An event is disregarded if the difference between the maximum and minimum peak slip rates during the event is less than 15% of the threshold velocity (0.2 m/s) to eliminate minor fluctuations in slip rate.

A 'system-size earthquake' is defined as an event that ruptures a length greater than 10 km (i.e., the entire seismogenic zone), while all other events are denoted 'partial rupture events' hereafter. A 'leading foreshock' is defined as the first partial rupture event in a sequence that eventually leads to a system-size earthquake.

2.4 Assessing the Level of Complexity

To quantitatively evaluate the degree of complexity across different models, we introduce a 'complexity score' based on three aspects of slip history: 1) how widely the hypocenters of system-size earthquakes are distributed as a function of depth, 2) the periodicity of the sequence, and 3) whether partial ruptures exist and if so, how diverse their sizes are. Each aspect is scored between 0 and 1, and the combined complexity score, the sum of all three metrics, ranges from 0 to 3.

The complexity score for hypocenter depth heterogeneity of system-size earthquakes is computed based on the histogram of hypocenter depths of system-size earthquakes. We count the number of bins n along depth (0.5 km interval) that contain at least one system-size earthquake hypocenter. To ensure a score of zero when all events occur at the same depth, we subtract 1 from the bin count ($n-1$). The respective score is then $(n-1)/(N-1)$, where N is the maximum value of n in all of the tested models.

The complexity score for periodicity is computed from the standard deviation of indices for the nearest system-size events with hypocenter depths less than 0.5 km apart. This standard deviation is normalized to 1 to provide the final score.

Lastly, the complexity score for heterogeneity in partial rupture events is computed from the standard deviation of rupture lengths among partial rupture events. If no partial rupture events are present, the score is assigned a value of zero, and the resulting score is normalized to 1.

3 Results

3.1 Models with Stress and Friction Heterogeneity

We explore a range of heterogeneities to yield a seismic cycle model with realistic variability in both event size and hypocenter depth distribution. A summary of all the models mentioned in this study is provided in Table 2. Using the aging law, we find that neither heterogeneity in any single parameter (Figs. 2a & 3) nor the presence of a low-rigidity fault zone (Fig. 4) alone is sufficient to introduce the desired complexity, with combined complexity score being less than 1 (Fig. 8). Models with heterogeneity in any single parameter exhibit characteristic cycles and hypocenters located only at the periphery of the seismogenic zone, similar to results from models that do not assume any fractal heterogeneity (e.g., Lapusta & Rice, 2003; Lindsey & Fialko, 2016). This lack of complexity in earthquake cycles is consistent across all single-parameter heterogeneity models with varying fractal profiles (Figs. 2a & 3), except for the model with a varying $(a-b)$ profile (2b). We also tested models in which normal stress increases with depth with superimposed fractal heterogeneity (Fig. 3c), but the cycles remained repeatable, with nucleation limited to the bottom edge of the seismogenic zone, where the critical nucleation size (L_∞, Eq. (5)) is the smallest.

Introducing an $(a-b)$ profile with VS patches within the seismogenic VW region (Fig. 1c) gives rise to earthquakes that nucleate at various depths within the seismogenic zone, rather than only at its periphery (Figs. 2b-d). Earthquakes nucleate at the boundaries of VS patches, where the stressing rate is increased due to creep on VS patches. Combining this $(a-b)$ profile with heterogeneity in other model parameters introduces a greater diversity in the slip modes. For example, heterogeneity in both stress and strength, along with a small $\overline{D_{RS}}$ value of 2 mm, produces slow slip events, partial rupture events, and system-size earthquakes (Fig. 2c). The hypocentral depths of the system-size events are well-distributed throughout the seismogenic zone. However, the sequence is still periodic, with a fixed nucleation depth for system-size earthquakes.

We confirm that the ratio of the width of the seismogenic zone to the critical nucleation size (i.e., W/L_∞) affects the system's complexity, including its periodicity (i.e., Barbot, 2019; Cattania, 2019). For instance, the two models in Figures 2c (model NRD) and 2d (model A2) share the same set of parameters, except that the model shown in Figure 2d has a lower bulk rigidity (μ = 32 GPa in NRD vs. μ = 20 GPa in A2), resulting in a smaller L_∞ and a higher value of W/L_∞. As expected, the model with a higher W/L_∞ value produces aperiodic sequences with a wide range of hypocenter depths and a diverse spectrum of ruptures. We discuss the control of W/L_∞ on the slip complexity in more detail in Section 4.2.

3.2 Models with a Low Rigidity Fault Zone

We performed additional seismic cycle simulations adding a low-rigidity region surrounding the fault, as an analogy to damage zones developing near active faults (e.g., Chester et al., 1993; Fialko et al., 2002; Y. Huang et al., 2014; Gabriel et al., 2024). We include a rectangular low-rigidity fault zone (with rigidity μ_{FZ}), 500 m wide and 10 km deep, which tapers at the bottom end as a semi-circle with a 500 m radius (Fig. 1a).

We find that the presence of the low-rigidity fault zone has minimal impact on earthquake sequences within the model space considered in this study, regardless of the rigidity contrast. Without the inclusion of fractal heterogeneities in the initial dynamic parameters, the low-rigidity fault zone alone results in partial rupture events and system-size earthquakes, but the sequence remains cycle-invariant, with hypocenters located only at the bottom of the seismogenic zone.

When the low-rigidity fault zone (μ_{FZ} = 20 GPa & μ = 32 GPa) is included in the models with fractal heterogeneities (model NDFZ; Fig. 4a), it reduces both the peak slip rate and the recurrence interval of the system-size earthquakes compared to a model with a lower rigidity in the entire bulk (μ = 20 GPa; model ND; Fig. 4b), as reported by previous studies (Abdelmeguid et al., 2019; Flores-Cuba et al., 2024; Kaneko et al., 2011). However, the low-rigidity fault zone model still exhibits periodic cycles and does not introduce variability in hypocenter depth.

Nevertheless, we find that the presence of the low-rigidity fault zone promotes pulse-like propagation of rupture, some with back-propagating rupture fronts (Beroza & Spudich, 1988; Ding et al., 2024; Flores-Cuba et al., 2024; Idini & Ampuero, 2020). Multiple slip pulses are clearly visible in the NDFZ model (Fig. S1a) in contrast to the ND model which exhibits crack-like ruptures (Fig. S1b). After ~ 7 s after the start of a system-size earthquake in the NDFZ model, one of the slip pulses seems to propagate back towards the hypocenter and re-ruptures the nearly healed part (i.e., $V < 1$ cm/s) of the fault (white-colored area in Fig. S1). We discuss back-propagating slip pulses in more detail in Section 4.3.

3.3 Features of Complex Aging Law Models

We obtain the most complex aging law model (Figs. 2d & 5) by combining heterogeneity in all three parameters (Figs. 1b-d) with $\mu = 20$ GPa and $\overline{D_{RS}} = 2$ mm. In this model, system-size earthquakes are consistently preceded by a cascade of partial rupture events. This model has a median W/L_∞ of 66 with a maximum of 251 (note that we have a depth-varying W/L_∞ ratio due to the fractal distribution of parameters). We run this model for 5,000 yr of simulation time and use it as the most complex aging law model throughout the study (hereafter denoted as 'A2', where 'A' stands for aging law and '2' stands for the $\overline{D_{RS}}$ of 2 mm).

The A2 model also produces spontaneous deep and shallow slow slip events (SSEs; Wei et al., 2009; Beroza & Ide, 2011; Rousset et al., 2019; Vavra et al., 2024) following system-size earthquakes or partial rupture events (Figs. 5a & 6). Deep SSEs occur after both sequences of partial rupture events and sequences that eventually lead to a system-size earthquake. The deep SSEs spatially coincide with a small VW patch embedded within the deep VS zone. This suggests that instability is initiated at the VW patch but fails to grow into a runaway seismic rupture due to the VS barriers located above and below. The recurrence time of the deep SSEs is generally shorter following system-size earthquakes (Fig. 6c). Shallow SSEs occur only after a sequence of partial rupture events, presumably to relax the stress induced by the preceding sequence. The peak slip rate of the shallow SSEs is an order of magnitude lower than that of the deep SSEs (Figs. 6a-b). Both shallow and deep SSEs are often followed by a sequence of partial rupture events, similar to the observation of aseismic slip preceding small to moderate earthquakes (e.g., Linde et al., 1988; L. Huang et al., 2024; Thurber, 1996; Thurber & Sessions, 1998).

3.4 Comparing Aging Law and Slip Law Models

We perform a suite of simulations to assess the effect of using different evolution laws. The model assuming slip law is shown in Figure 7a. This model uses the same set of parameters as used in the A2 simulation but with an increased $\overline{D_{RS}}$ of 10 mm to reduce the computational burden (see Supplementary Section S1). The modeled earthquake sequence (denoted as S10, where 'S' stands for slip law) is characterized by the repetition of a partial rupture event at the base of the seismogenic zone followed by a system-size earthquake in the middle of the seismogenic zone ($\sim$7 km depth). Periodic earthquake sequences and a lack of smaller earthquakes are observed in model S10, as noted in previous studies that considered the effects of slip law (e.g., Rice & Ben-Zion, 1996; Rubin, 2008).

Since the input parameters of the S10 model are not identical to those of the A2 model, we produce a new aging law model using $\overline{D_{RS}} = 10$ mm (denoted as 'A10' model hereafter; Fig. 7b), for direct comparisons among different evolution laws. The A10 and A2 models differ only in the magnitude of $\overline{D_{RS}}$ (10 mm vs. 2 mm).

The A10 model shows more complex earthquake sequences with multiple partial rupture events preceding system-size earthquakes compared to the 'equivalent' slip law model (S10). In the A10 model, a sequence of partial rupture events is connected by a prolonged aseismic slip within the sequence, leading to a system-size earthquake. Due to this prolonged aseismic slip, each foreshock-mainshock sequence in the A10 model lasts for about 5 months on average, much longer compared to ∼10 seconds in the S10 model or ∼10 hours in the A2 model.

We find that the aging law (A10 model) tends to produce larger static stress drops and peak slip rates during its system-size events compared to the slip law (S10 model), although their differences are rather small: The A10 model and the S10 model have average stress drops of ∼ 7 MPa and ∼ 5 MPa, respectively, and average peak slip rates of ∼ 3.4 m/s and ∼ 3.2 m/s. Differences in stress drops and peak slip rates between models using aging- and slip laws are consistent with results from previous studies (Hawthorne & Rubin, 2013; He et al., 2003; Perfettini & Ampuero, 2008; Pignalberi et al., 2024); we provide a more detailed comparison in Section 4.4.

4 Discussion

4.1 Variability in the Hypocenter Depth

Contrary to the predictions of classic models of seismic cycles on RSF faults, which limit earthquake nucleation to the edges of the VW layer representing the seismogenic zone (Lapusta & Rice, 2003; Rice, 1993; Tse & Rice, 1986), natural faults exhibit a wide range of hypocenter depths (Melgar et al., 2023; Ross et al., 2020; Waldhauser & Schaff, 2008). In particular, in California, most earthquakes nucleate in the middle, rather than at the edges, of the seismogenic zone (Jin & Fialko, 2020).

The models presented here replicate such diverse hypocenter depths only when we introduce VS patches within the seismogenic zone (Figs. 1c & 2b-d). This variability arises because stress concentrates at the VS-VW transitions due to creep in the VS patch (e.g., Lapusta & Rice, 2003; Lindsey & Fialko, 2016). These transitions between VS and VW also facilitate the spontaneous occurrence of deep SSEs.

Previous studies utilizing multiple VS patches within a seismogenic fault successfully reproduced a wide spectrum of slip behavior and realistic foreshock migration patterns (Ito & Kaneko, 2023; Luo & Ampuero, 2018; Song & McLaskey, 2024). Such small-scale heterogeneity with different rheological properties coincides with intermediate behavior (between fully locked and fully creeping) inferred from geodetic observations

In the context of the 2D antiplane strain models presented here, no heterogeneity other than that in the $(a - b)$ parameter is capable of producing a broad distribution of event hypocenters. Even in models with partial rupture events, we find that stress heterogeneity generated by partial ruptures is insufficient to nucleate system-size earthquakes within the seismogenic zone, rather than at its edges (e.g., Figs. 2a & 3). This limitation persists even in models that show variable rupture extent and realistic frequency-magnitude relationships (e.g., Cattania, 2019). In contrast, such variability in nucleation depths is frequently observed in 3D models incorporating material heterogeneity (Galvez et al., 2020; Hillers et al., 2006; Jiang & Lapusta, 2016; Perez-Silva et al., 2022) or complex fault geometry (Perez-Silva et al., 2022; Ozawa & Ando, 2021; Yin et al., 2023). (e.g., B. Zhao et al., 2022).

4.2 Control of W/L_∞ on the Slip Complexity

The model results in this study confirm that a larger W/L_∞ encourages the emergence of quasi-chaotic cycles (e.g., models NRD vs. A2). We systematically compare maximum and median values of W/L_∞ with the complexity scores (Section 2.4) across all aging law models (Fig. 8).

Overall, the maximum W/L_∞ ratio correlates well with the combined complexity score (Fig. 8d). We also observe that the A2 model, the most complex model in this study, shows the largest W/L_∞ ratio in both maximum and median values. A larger W/L_∞

ratio tends to increase the diversity in partial rupture events (Fig. 8c), while having little impact on the periodicity (Fig. 8b) and the hypocenter depth heterogeneity of system-size earthquakes (Fig. 8a).

However, a larger W/L_∞ ratio does not always lead to a more complex model. For example, the N4 model (pentagons in Fig. 8) has a larger median W/L_∞ ratio than the NRD model (squares in Fig. 8) and higher median and maximum W/L_∞ ratios than the NDFZ (plus signs in Fig. 8) and ND (cross signs in Fig. 8) models. Yet, model N4 is entirely periodic, producing only system-size earthquakes that nucleate at a fixed depth, and has a significantly lower combined complexity score of zero compared to models NRD (0.8), ND (0.3), and NDFZ (0.3). This lack of smaller earthquakes in model N4, despite the higher W/L_∞ ratio compared to models NDFZ and ND, is likely related to the model setup differences: model N4 incorporates a depth-dependent effective normal stress that reaches $\sim$ 200 MPa at the base of the seismogenic zone, unlike the uniform effective normal stress of 50 MPa within the seismogenic zone in models NDFZ and ND. It is expected that depth-dependent normal stress favors nucleation at the base of the seismogenic zone but adds little to complexity (e.g., Zhang et al., 2006).

The comparison between models N4 and NDFZ/ND shows that the W/L_∞ ratio may not serve as an absolute criterion for predicting the degree of complexity among models with substantially different setups. Previous studies emphasizing the control of W/L_∞ ratio on complexity often utilize simple setups, such as depth-independent stress values (e.g., Cattania, 2019), or perform isolated parameter searches, such as changing the D_{RS} value while fixing other parameters (e.g., Barbot, 2019; Lapusta & Rice, 2003). These approaches offer systematic insights into how W/L_∞ affects rupture behavior under a given specific setup. However, the results presented here challenge the notion of a 'universal threshold' W/L_∞ ratio that is universally applicable to various models. Instead, we show that similar W/L_∞ ratios may produce varying degrees of complexity depending on model configurations. A lack of correlation between higher W/L_∞ ratios and increased complexity has also been noted in previous 2D antiplane simulations (e.g., Abdelmeguid et al., 2019).

In addition, we evaluate whether the observed complexity in model A2 stems from a high maximum W/L_∞ ratio or from heterogeneous fault properties. We perform a simulation with a constant high value of W/L_∞ of 251, the same as the maximum W/L_∞ value in the A2 model, but with homogeneous input parameters (Fig. S2). The homogeneous model generates both system-size and partial rupture events, but their hypocenter depths are restricted to the base of the seismogenic zone and the cycle remains periodic. This result highlights the role of material heterogeneity and shows that the W/L_∞ ratio is not a sole predictor of the system complexity.

4.3 The Effect of a Low-Rigidity Fault Zone

We found that the presence of a low-rigidity fault zone does not increase the complexity of the earthquake cycle (compare models NDFZ and ND). This finding is in line with the comprehensive parameter search by Nie and Barbot (2022), who concluded that low-rigidity fault zones contribute to complexity only by decreasing the nucleation size. Models with and without such low-rigidity fault zones are indistinguishable when they share a similar W/L_∞ ratio.

As also noted by Nie and Barbot (2022), the insensitivity of rupture behavior to the presence of a low-rigidity fault zone may stem from the absence of complex wave interaction within the fault zone in quasi-dynamic simulations. Fully dynamic models, however, show significant changes in rupture behavior, such as a broader depth range of earthquake hypocenters, when low-rigidity fault zones are present (Y. Huang & Ampuero, 2011; Y. Huang et al., 2014; Thakur et al., 2020). Similar effects are observed in models incorporating off-fault plasticity or damage rheology (Niu et al., 2024; Thakur & Huang, 2021; C. Zhao et al., 2024).

Back-propagating slip pulses spontaneously emerge in the quasi-dynamic model with a low-rigidity fault zone presented in this study. Although back-propagating ruptures have often been associated with dynamic effects such as free-surface reflection (Burridge & Halliday, 1971; Ding et al., 2024; Kaneko & Lapusta, 2010; Y. Huang et al., 2012), seismic wave interference (Ding et al., 2024; Flores-Cuba et al., 2024), or rapid coseismic weakening and healing (Gabriel et al., 2012), they have also been previously observed in quasi-dynamic simulations (e.g., Barbot, 2021; Cattania, 2019; Yingdi & Ampuero, 2017). Idini and Ampuero (2020) explains the existence of such back-propagating fronts in quasi-dynamic simulations by deriving a static stress transfer kernel in relation to the nearest-neighbor model, such as the Burridge-Knopoff model (Burridge & Knopoff, 1967). These analytical results predict the prevalence of slip pulses as the damage level within a low-rigidity fault zone increases. The crack-to-pulse transition leaves slip deficits, which gives rise to back-propagating fronts (Flores-Cuba et al., 2024).

Importantly, the back-propagating slip pulses are not exclusive to highly complex models. For example, the NDFZ model shows cycle-invariant rupture characteristics with a single earthquake per cycle (combined complexity score of 0.3), indicating that such pulses can arise in relatively simple setups.

4.4 Different Rupture Styles of the Aging Law and the Slip Law

In section 3.4, we observe key differences between models using the aging law (A10 model) and the slip law (S10 model). The slip law model tends to produce: (1) super cycles of shorter duration, consisting of fewer earthquakes per cycle, (2) smaller average static stress drop, and (3) smaller peak slip rates during system-size earthquakes.

The rapid cascade of earthquake sequences with fewer smaller earthquakes in the slip law model is consistent with the highly non-linear nature of the slip law. The slip law shows slower growth of fracture energy during rupture acceleration, allowing instability to develop over a smaller length scale (i.e., smaller critical nucleation size) and facilitating easier rupture propagation across the entire fault (Ampuero & Rubin, 2008). Previous studies have shown that the slip law can accommodate unstable slip regardless of the stiffness of the system (Gu et al., 1984; Ranjith & Rice, 1999), particularly when subjected to stress perturbations (Helmstetter & Shaw, 2009; Perfettini & Ampuero, 2008).

While smaller static stress drops under the slip law are well-documented (Hawthorne & Rubin, 2013; He et al., 2003), peak slip rate comparisons between slip and aging laws have yielded varying conclusions across different models. For example, using the slip law, Perfettini and Ampuero (2008) report higher peak slip rates under finite stress perturbation, while He et al. (2023) observe the opposite within a weakening zone during the nucleation process. These discrepancies may arise from differences in model setups, such as the spring-slider system or homogeneous frictional properties, and correlations between kinematic parameters may depend on the local heterogeneity of dynamic parameters (Schliwa et al., 2024; Schmedes et al., 2010; Vyas et al., 2023). To the best of our knowledge, this study presents the first systematic comparison of rupture characteristics for the aging and slip laws under more realistic conditions, incorporating fractal heterogeneity in stress and material properties.

4.5 Transition from Aperiodic to Cycle-Invariant Regimes

We find that the earthquake sequences, even in the most complex model in this study (A2), eventually become more regular if the simulations are run for a sufficiently long time (Fig. 9). In the A2 model, the transition occurs after ~ 1750 yr of simulation time, equivalent to 23 system-size earthquakes. This transition from aperiodic to periodic cycles implies that the initial complexity in the modeled earthquake sequences might represent a prolonged spin-up phase and that it might take tens of cycles to completely eliminate the effect of initial conditions.

The loss of complexity in the later stage of the simulation fundamentally questions the possibility of obtaining aperiodic earthquake sequences in 2D anti-plane strain quasi-dynamic models. Previous studies that found non-characteristic (i.e., aperiodic) regimes often analyzed only a few hundred years, or equivalently, several system-size cycles, and it is not clear if the reported complexity persists over much longer time intervals (Cattania, 2019; Ito & Kaneko, 2023; Molina-Ormazabal et al., 2023; Nie & Barbot, 2022).

A more sustainable aperiodic behavior of modeled earthquake sequences may be achieved by explicitly accounting for the rough fault geometry (e.g., Cattania & Segall, 2021; Tal & Gabrieli, 2024), rather than approximating the effects of fault roughness (e.g., by applying spatially variable normal stress), as the topography of the fault surface perpetually introduces heterogeneity in stress to the system (Dunham et al., 2011; Fang & Dunham, 2013; Romanet et al., 2020). Whether complexity can be sustained beyond the timespans reported here in 2D anti-plane strain quasi-dynamic simulations, and under what conditions, remains an open question for future research.

After the 1750-year transition to a periodic sequence (including 2 repeating cycles), we observe repeating earthquakes ('repeaters'; Uchida & Bürgmann, 2019), such as the two unlabeled events preceding event 246 and event 265 in Figure S3. These repeaters occur at a depth of 11.36 km with a recurrence interval of 152 yr. The repeaters in this model show a significantly smaller slip ($\sim$ 0.3 m) than that expected from the creeping velocity at the VS area surrounding the repeater asperity ($\sim$ 5 m), similar to observations of natural repeaters (e.g., Chen et al., 2007; Nadeau & Johnson, 1998). These results suggest that caution should be exercised when using repeaters to infer local creep rates (Turner et al., 2024).

5 Conclusions

We extensively explore the effects of various types of heterogeneities on generating non-characteristic earthquake cycles with considerable complexity in rupture size and hypocenter depth distributions in 2D quasi-dynamic rate-and-state friction simulations. Using the aging law, we find that a broad spectrum of fault slip, including both system-size and partial ruptures, occurs only when multiple fractal heterogeneities in both stress and strength parameters are introduced conjointly. Velocity-strengthening patches are critical for enabling depth-variable earthquake nucleation throughout the entire seismogenic zone due to elevated stressing rates at their margins.

The presence of a low-rigidity fault zone does not increase system complexity compared to homogeneous models with comparable W/L_∞ ratios. Nevertheless, a low-rigidity fault zone does promote pulse-like ruptures that occasionally back-propagate, re-rupturing the hypocentral area.

While the model with the most complex earthquake sequence exhibits the largest W/L_∞ ratio, different models with similar W/L_∞ ratios show varying degrees of complexity. This result highlights that fault slip complexity can be highly model-dependent, and thus, caution is needed when using W/L_∞ as a predictive metric.

The most complex aging law model presented here features system-size earthquakes with a range of hypocentral depths, which are consistently preceded by a cascade of partial ruptures, as well as shallow and deep slow slip events. In addition, this model reproduces other observed characteristics of natural faults, such as repeating earthquakes and aseismic transients preceding small-to-moderate-size earthquakes. However, even this most complex sequence transitions from aperiodic to periodic cycles after thousands of years, implying that effects of initial conditions in cycle simulations may be more persistent than previously thought.

Finally, we compare earthquake sequences under aging and slip law assumptions. The slip law models produce shorter-duration super cycles consisting of fewer earthquakes per cycle, smaller average static stress drops, and lower peak slip rates during system-size earthquakes.

Table 1. Base values for the parameters used in the seismic cycle models using *Tandem*. z is depth in kilometers.

Symbol	Parameter	Value
a	Rate-and-state parameter, direct effect	Varies (see Fig. 1c)
b	Rate-and-state parameter, evolution effect	0.019
D_{RS}	Characteristic state evolution distance	4 mm
f_0	Reference coefficient of friction	0.6
V_0	Reference slip rate	10^{-6} m/s
V_{init}	Initial slip rate	10^{-9} m/s
V_{pl}	Plate loading rate	10^{-9} m/s
σ_n^0	Background effective normal stress	50 MPa (see Fig. 1b)
τ^0	Background shear stress	Varies (see Fig. 1b)
ν	Poisson's ratio	0.25
W	Seismogenic zone width*	$\sim$ 10 km
L_f	Rate-and-state fault length	24 km

* May slightly vary due to fractal heterogeneity (see Section 2.2).

Table 2. List of all models presented in this study. Horizontal dash indicates the model does not incorporate fractal variation in the given parameter (or does not include a low-rigidity fault zone) and the parameter follows the base value shown in Table 1. Models are named by the combination of the type the fractal heterogeneities included in the model (N: effective normal stress, R: rate-and-state parameter $(a-b)$, and D: characteristic state evolution distance) or the presence of a low-velocity fault zone (FZ). (CCS: Combined Complexity Score.)

Model Name	$\overline{\sigma_n^0}$ [a] [MPa]	$\overline{a-b}$ [b]	$\overline{D_{RS}}$ [mm]	λ_{min} [km]	λ_{max} [km]	μ [GPa]	μ_{FZ} [GPa]	CCS
N1	50	-	-	0.5	2.5	32	-	0.3
R	-	-0.004	-	0.5	2.5	32	-	1.0
NRD	50	-0.004	2	0.5	2.5	32	-	0.9
N2	50	-	-	0.75	5	32	-	0.0
N3	50	-	-	0.2	1.0	32	-	0.0
N4 [c]	258	-	-	0.5	2.5	20	-	0.0
NDFZ	50	-	2	0.5	2.5	32	20	0.3
ND	50	-	2	0.5	2.5	20	-	0.3
A2	50	-0.004	2	0.5	2.5	20	-	2.8
S10	50	-0.004	10	0.5	2.5	20	-	0.3
A10	50	-0.004	10	0.5	2.5	20	-	0.7

[a] Value below 2 km.
[b] Value within the velocity-weakening seismogenic zone (2 km - 12 km).
[c] Depth-dependent effective normal stress model.

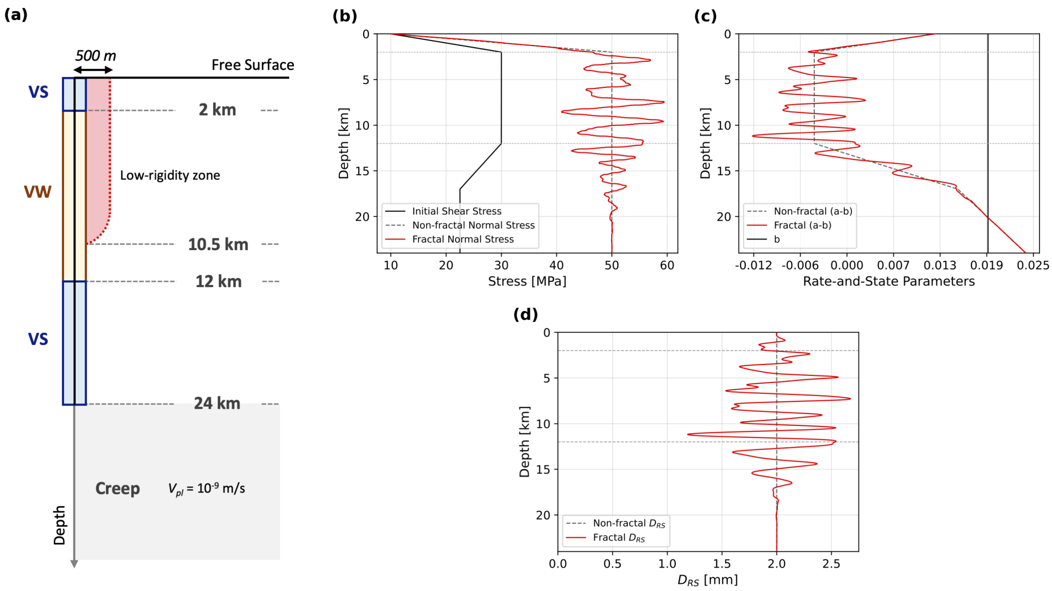

Figure 1. (a) Sketch of the model geometry for the seismic cycle simulations using *Tandem*. The rate-and-state fault (black vertical line) includes a central velocity-weakening zone (yellow) surrounded by shallow and deep velocity-strengthening zones (blue). The bottom creep zone governed by the constant loading rate (V_{pl}) is shaded in grey. The red-shaded area indicates the spatial extent of a low-rigidity fault zone. As the model represents a perfectly symmetric vertical strike-slip fault, we model only one side of the domain. (b-d) Self-affine fractal distributions of (b) initial effective normal stress, (c) rate-and-state parameters, and (d) characteristic state evolution distance, that parameterize the most complex aging law model (A2 model). The fractal distributions of all three parameters share the same limiting wavelengths of λ_{min} = 500 m and $\lambda_{max} = 2.5$ km.

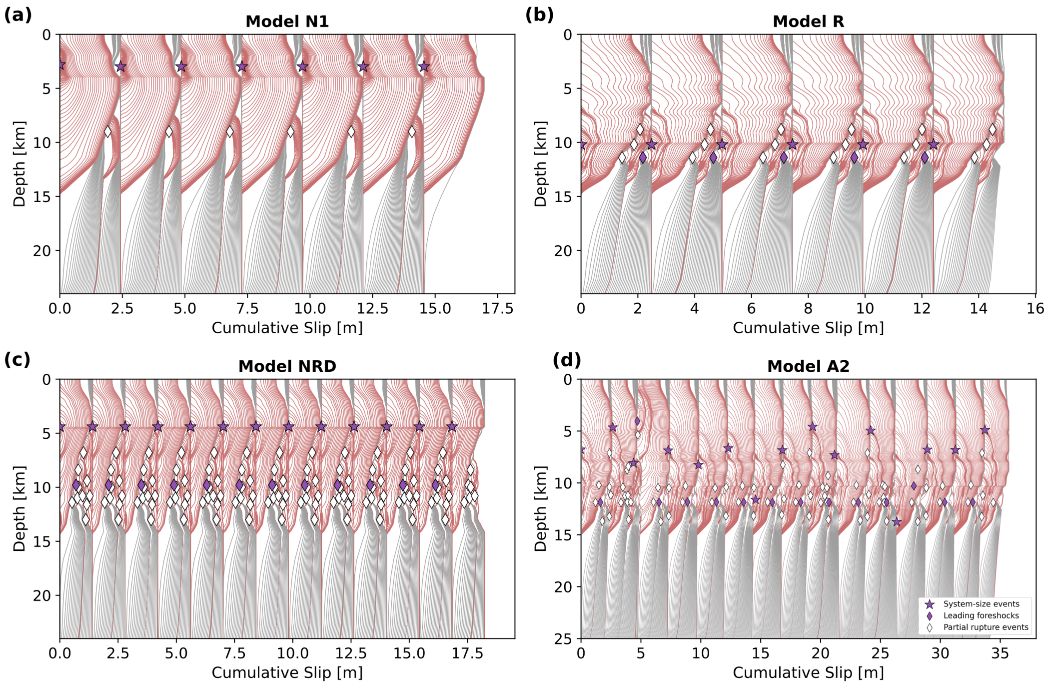

Figure 2. Cumulative slip evolution along the fault in exemplary seismic cycle simulations with initial stress and strength heterogeneity. (a) Seismic cycle model with heterogeneity only in initial effective normal stress using the fractal distribution shown in Figure 1b (model N1). (b) Seismic cycle model with heterogeneity only in $(a - b)$ parameter using the fractal distribution shown in Figure 1c, featuring velocity-strengthening patches embedded within the seismogenic layer (model R). (c-d) Models with heterogeneity in all three parameters using the fractal distributions shown in Figures 1b-d, but with different shear moduli of (c) 32 GPa (model NRD) and (d) 20 GPa (model A2). All models show the cumulative slip omitting the first 200 yr of spin-up time. The model in (d) shows the first 1,353 yr of a 5,000-year simulation. Pink contours, drawn every 0.5 s, show the coseismic evolution of slip, while grey contours, plotted every 2 yr, show the longer-term evolution of slip. Purple stars, purple diamonds, and white diamonds indicate the hypocenter locations of system-size earthquakes, leading foreshocks, and partial rupture events, respectively.

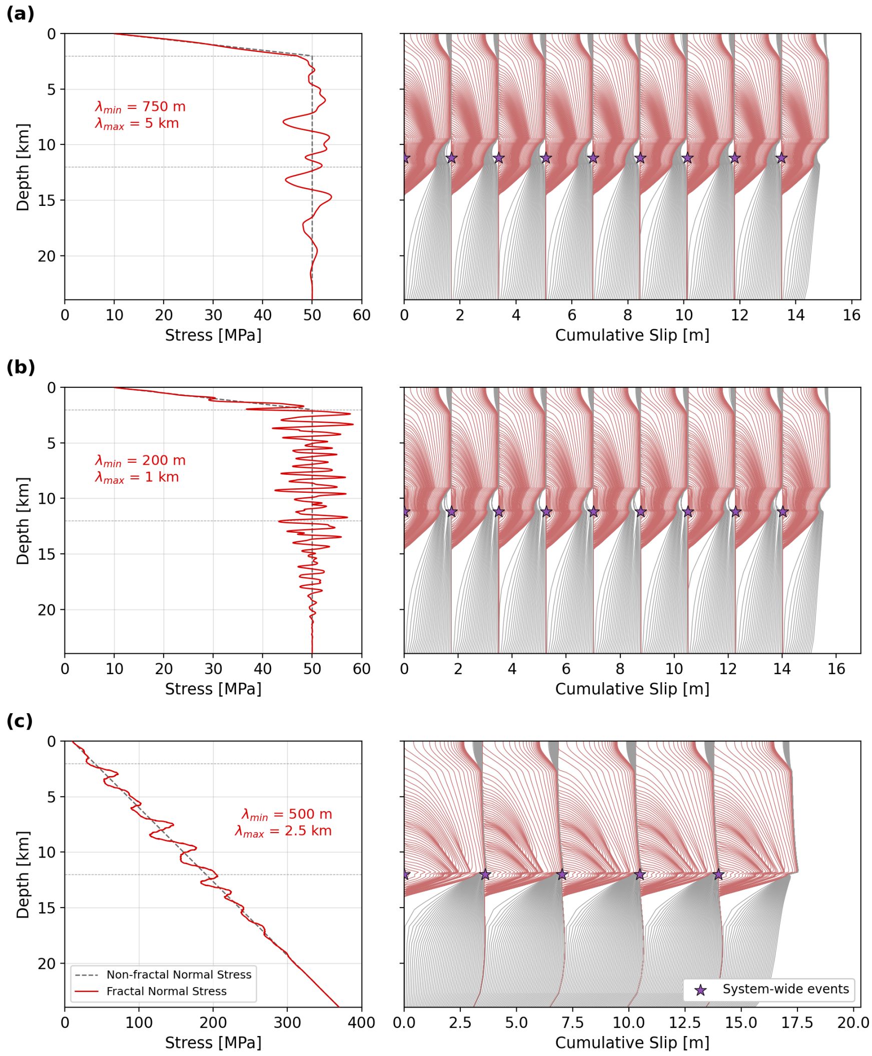

Figure 3. Seismic cycle models with heterogeneity only in initial effective normal stress. (a-b) Seismic cycle models with fractal heterogeneity using different limiting wavelengths of the fractal distribution (λ_{min} and λ_{max}): (a) λ_{min} = 750 m and λ_{max} = 5 km (model N2) and (b) λ_{min} = 200 m and λ_{max} = 1 km (model N3). (c) Seismic cycle model in which normal stress increases with depth with superimposed fractal heterogeneity of λ_{min} = 500 m and λ_{max} = 2.5 km (model N4). The left columns show the fractal distribution of the initial effective normal stress and the right columns show the corresponding cumulative slip evolution along the fault. All models show the cumulative slip omitting the first 200 years of spin-up time. Pink contours, drawn every 0.5 s, show the coseismic evolution of slip, while grey contours, plotted every 2 yr, show the longer-term evolution of slip. Purple stars, purple diamonds, and white diamonds indicate the hypocenter locations of system-size earthquakes, leading foreshocks, and partial rupture events, respectively.

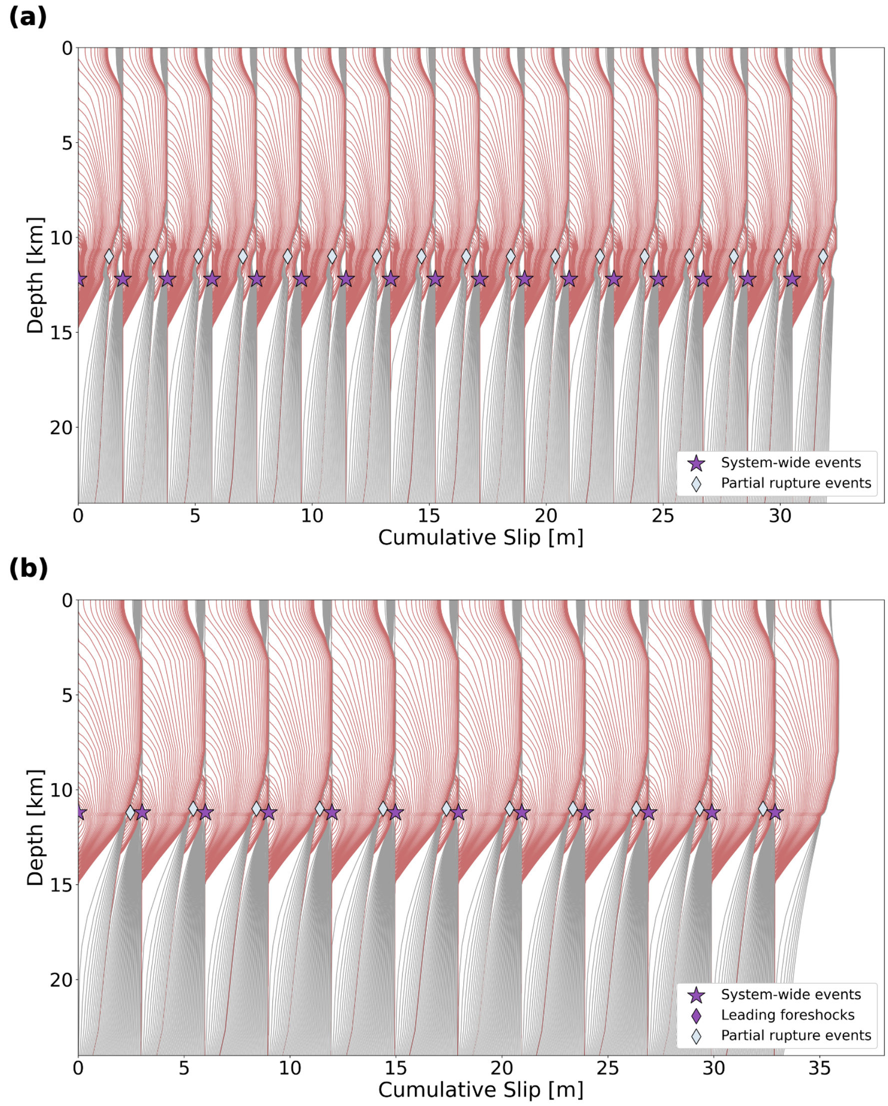

Figure 4. Comparison of seismic cycle models with and without a low-rigidity fault zone surrounding the fault (red shaded area in Fig. 1a). (a) Model NDFZ, featuring a low-rigidity fault zone (μ_{FZ} = 20 GPa) embedded in the bulk with μ = 32 GPa. (b) Model ND, featuring a lower-rigidity bulk with μ = 20 GPa but without a low-rigidity fault zone. Both models share fractal heterogeneities in the initial effective normal stress and characteristic state evolution distance shown in Figures 1b and 1d. All models show the cumulative slip omitting the first 200 years of spin-up time. Pink contours, drawn every 0.5 s, show the coseismic evolution of slip, while grey contours, plotted every 2 yr, show the longer-term evolution of slip. Purple stars, purple diamonds, and white diamonds indicate the hypocenter locations of system-size earthquakes, leading foreshocks, and partial rupture events, respectively.

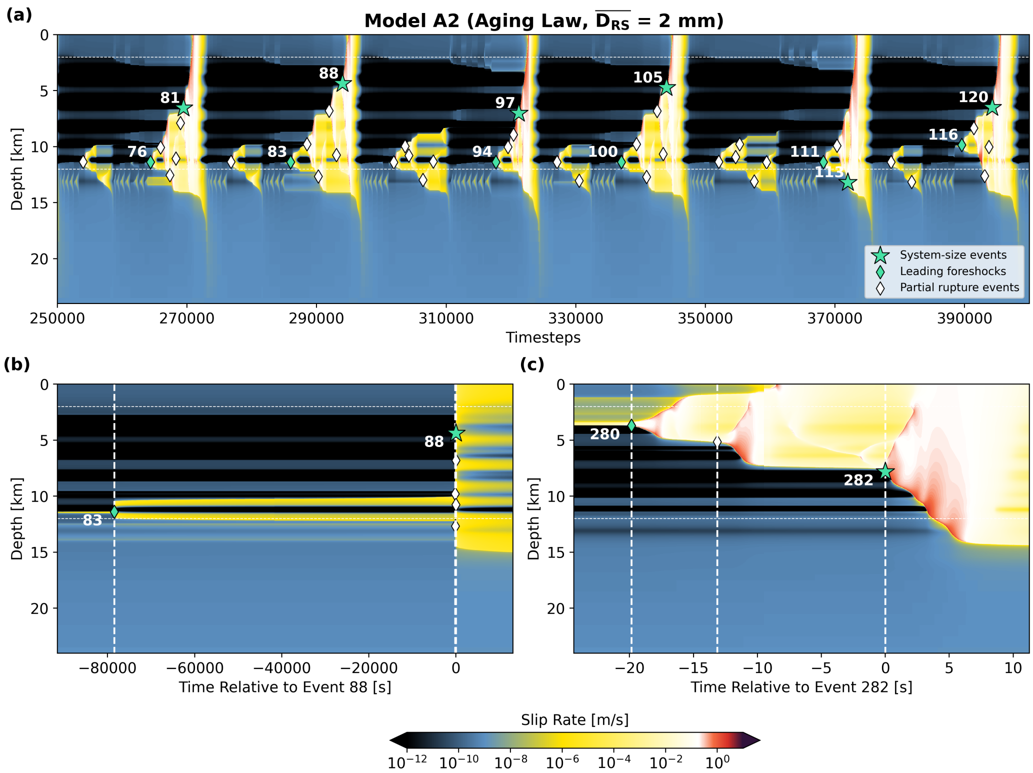

Figure 5. Spatiotemporal evolution of slip rate of the most complex aging law seismic cycle model (A2; see Section 3.3). (a) The slip rate evolution for every time step between 745 yr and 1,180 yr of simulation time. (b-c) Zoom-in of two foreshock-mainshock sequences with different migration patterns (deep-to-shallow vs. shallow-to-deep) and durations (22 h vs. 20 s). Green stars, green diamonds, and white diamonds indicate the hypocenter locations of system-size earthquakes, leading foreshocks, and partial rupture events, respectively. Numbers next to the markers indicate the event number.

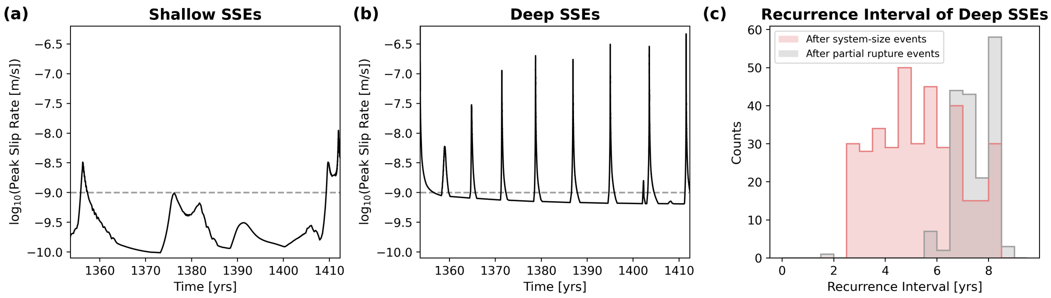

Figure 6. Slow slip events (SSEs) observed in the most complex aging law seismic cycle model (A2 model). (a-b) Peak slip rates of the shallow (<5 km) and the deep (10 km - 20 km) SSEs. Grey dashed lines mark the constant plate loading rate (V_{pl}). (c) Recurrence interval of the deep SSEs following system-size earthquakes (pink) and partial rupture events (grey).

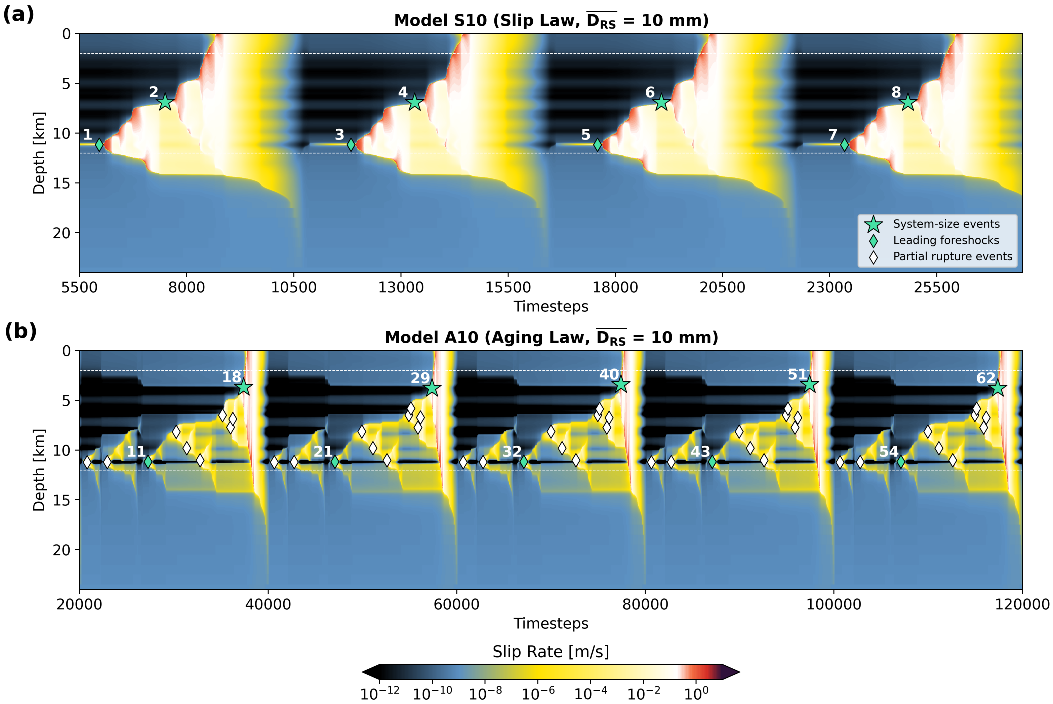

Figure 7. Comparison of spatiotemporal evolution of slip rate of models using (a) slip law (S10 model) and (b) aging law (A10 model) sharing the same input parameters (see Section 3.4). Event numbering starts from a non-zero value since we only show the spun-up phase of the models, i.e., after 200 yr of simulation time. Green stars, green diamonds, and white diamonds indicate the hypocenter locations of system-size earthquakes, leading foreshocks, and partial rupture events, respectively.

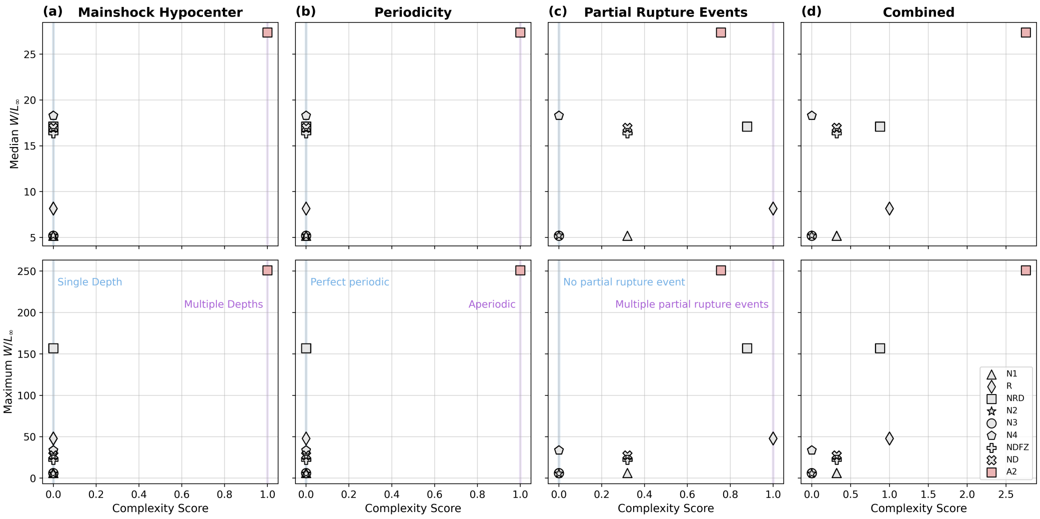

Figure 8. Correlation between the complexity score (see Section 2.4) and W/L_∞ ratio among different models using aging law. The top row shows the correlation with the median W/L_∞ ratio while the bottom row shows the correlation with the maximum W/L_∞. (a-c) Individual complexity scores for (a) hypocenter depth heterogeneity of system-size earthquakes, (b) periodicity, and (c) heterogeneity in partial rupture events. (d) Combined complexity score, the sum of the three individual complexity scores, ranging from 0 to 3. See Table 2 for model name definition.

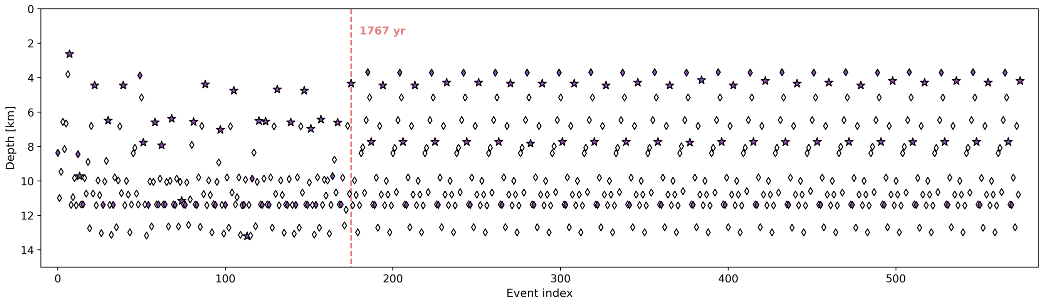

Figure 9. Hypocenter depth distribution for all earthquakes in the most complex aging law seismic cycle model (A2 model). A transition from an aperiodic to a cycle-invariant regime occurs after ∼1,750 yr of simulation time (pink dashed line). Purple stars, purple diamonds, and white diamonds indicate the hypocenter locations of system-size earthquakes, leading foreshocks, and partial rupture events, respectively.

6 Open Research

All data required for reproducing the *Tandem* seismic cycle models can be downloaded from the Zenodo repository, [redacted]. The open-source software *Tandem* is available at `https://github.com/TEAR-ERC/tandem`. We use dmay/seas-checkpoint branch (commit #1dc36db; `https://github.com/TEAR-ERC/tandem/tree/dmay/seas-checkpoint`) for aging law simulations and jyun/state-law branch (commit #5d5c63f; `https://github.com/TEAR-ERC/tandem/tree/jyun/state laws`) for slip law simulations.

Acknowledgments

We thank Prithvi Thakur, Camilla Cattania, and Junle Jiang for sharing their seismic cycle codes. We appreciate fruitful discussions with Eric Dunham. YF acknowledges support from NSF (EAR-1841273) and NASA (80NSSC22K0506). AAG and DAM acknowledge support from NSF, grants EAR-2121568 (MTMOD) and OAC-2311208 (Quakeworx). AAG acknowledges support from NSF, grants OAC-2139536 (LCCF-CSA) and EAR-2225286 (CRESCENT), the Southern California Earthquake Center (SCEC awards 24103, 24127, 22135, 23121, 22162), the European Union's Horizon 2020 Research and Innovation Programme (TEAR, grant number 852992), Horizon Europe (ChEESE-2P, grant number 101093038, DT-GEO, grant number 101058129, and Geo-INQUIRE, grant number 101058518), and NASA (80NSSC20K0495). We gratefully acknowledge the computing resources provided by the Institute of Geophysics of LMU Munich (Oeser et al., 2006). We also acknowledge the Gauss Center for Supercomputing e.V. (`https://www.gauss-centre.eu/`) for providing computing time on SuperMUC-NG, hosted at the Leibniz Supercomputing Center (`https://www.lrz.de/`), via project pn49ha.

References

Abdelmeguid, M., Ma, X., & Elbanna, A. (2019). A novel hybrid finite element-spectral boundary integral scheme for modeling earthquake cycles: Application to rate and state faults with low-velocity zones. *Journal of Geophysical Research: Solid Earth*, *124*(12), 12854–12881.

Abhyankar, S., Brown, J., Constantinescu, E., Ghosh, D., & Smith, B. F. (2014). *PETSc/TS: A modern scalable DAE/ODE solver library* (Preprint No. ANL/MCS-P5061-0114). Argonne National Laboratory.

Ampuero, J.-P., & Rubin, A. M. (2008). Earthquake nucleation on rate and state faults – Aging and slip laws. *Journal of Geophysical Research: Solid Earth*, *113*(B1).

Andrews, D., & Barall, M. (2011). Specifying initial stress for dynamic heterogeneous earthquake source models. *Bulletin of the Seismological Society of America*, *101*(5), 2408–2417.

Balay, S., Abhyankar, S., Adams, M. F., Brown, J., Brune, P., Buschelman, K., ... Zhang, H. (2019). *PETSc users manual* (Tech. Rep. No. ANL-95/11 - Revision 3.11). Argonne National Laboratory.

Balay, S., Gropp, W. D., McInnes, L. C., & Smith, B. F. (1997). Efficient management of parallelism in object oriented numerical software libraries. In E. Arge, A. M. Bruaset, & H. P. Langtangen (Eds.), *Modern software tools in scientific computing* (pp. 163–202). Birkhäuser Press.

Barbot, S. (2019). Slow-slip, slow earthquakes, period-two cycles, full and partial ruptures, and deterministic chaos in a single asperity fault. *Tectonophysics*, *768*, 228171.

Barbot, S. (2021). A spectral boundary-integral method for quasi-dynamic ruptures of multiple parallel faults. *Bulletin of the Seismological Society of America*, *111*(3), 1614–1630.

Barbot, S., Fialko, Y., & Bock, Y. (2009). Postseismic deformation due to the

Mw 6.0 2004 Parkfield earthquake: Stress-driven creep on a fault with spatially variable rate-and-state friction parameters. *Journal of Geophysical Research: Solid Earth*, *114*, B07405.
Barbot, S., Lapusta, N., & Avouac, J.-P. (2012). Under the hood of the earthquake machine: Toward predictive modeling of the seismic cycle. *Science*, *336*(6082), 707–710.
Bayart, E., Rubin, A. M., & Marone, C. (2006). Evolution of fault friction following large velocity jumps. In *Agu fall meeting abstracts* (Vol. 2006, pp. S31A–0180).
Beall, A., van den Ende, M., Ampuero, J.-P., Capitanio, F. A., & Fagereng, Å. (2022). Linking earthquake magnitude-frequency statistics and stress in visco-frictional fault zone models. *Geophysical Research Letters*, *49*(20), e2022GL099247.
Beeler, N., Tullis, T., & Weeks, J. (1994). The roles of time and displacement in the evolution effect in rock friction. *Geophysical research letters*, *21*(18), 1987–1990.
Ben-Zion, Y., & Rice, J. R. (1995). Slip patterns and earthquake populations along different classes of faults in elastic solids. *Journal of Geophysical Research: Solid Earth*, *100*(B7), 12959–12983.
Beroza, G. C., & Ide, S. (2011). Slow earthquakes and nonvolcanic tremor. *Annual review of Earth and planetary sciences*, *39*(1), 271–296.
Beroza, G. C., & Spudich, P. (1988). Linearized inversion for fault rupture behavior: Application to the 1984 Morgan Hill, California, earthquake. *Journal of Geophysical Research: Solid Earth*, *93*(B6), 6275–6296.
Burridge, R., & Halliday, G. (1971). Dynamic shear cracks with friction as models for shallow focus earthquakes. *Geophysical Journal International*, *25*(1-3), 261–283.
Burridge, R., & Knopoff, L. (1967). Model and theoretical seismicity. *Bulletin of the seismological society of america*, *57*(3), 341–371.
Cattania, C. (2019). Complex earthquake sequences on simple faults. *Geophysical Research Letters*, *46*(17-18), 10384–10393.
Cattania, C., & Segall, P. (2019). Crack models of repeating earthquakes predict observed moment-recurrence scaling. *Journal of Geophysical Research: Solid Earth*, *124*(1), 476–503.
Cattania, C., & Segall, P. (2021). Precursory slow slip and foreshocks on rough faults. *Journal of Geophysical Research: Solid Earth*, *126*(4), e2020JB020430.
Chen, K. H., Nadeau, R. M., & Rau, R.-J. (2007). Towards a universal rule on the recurrence interval scaling of repeating earthquakes? *Geophysical Research Letters*, *34*(16).
Chester, F. M., Evans, J. P., & Biegel, R. L. (1993). Internal structure and weakening mechanisms of the San Andreas fault. *Journal of Geophysical Research: Solid Earth*, *98*(B1), 771–786.
Cochard, A., & Madariaga, R. (1996). Complexity of seismicity due to highly rate-dependent friction. *Journal of Geophysical Research: Solid Earth*, *101*(B11), 25321–25336.
Dieterich, J. H. (1979). Modeling of rock friction: 1. Experimental results and constitutive equations. *Journal of Geophysical Research: Solid Earth*, *84*(B5), 2161–2168.
Dieterich, J. H. (1994). A constitutive law for rate of earthquake production and its application to earthquake clustering. *Journal of Geophysical Research: Solid Earth*, *99*(B2), 2601–2618.
Dieterich, J. H., & Kilgore. (1994). Direct observation of frictional contacts: New insights for state-dependent properties. *Pure and applied geophysics*, *143*, 283–302.
Ding, X., Xu, S., Fukuyama, E., & Yamashita, F. (2024). Back-propagating rupture:

Nature, excitation, and implications. *Journal of Geophysical Research: Solid Earth*, *129*(10), e2024JB029629.
Dunham, E. M., Belanger, D., Cong, L., & Kozdon, J. E. (2011). Earthquake ruptures with strongly rate-weakening friction and off-fault plasticity, part 2: Nonplanar faults. *Bulletin of the Seismological Society of America*, *101*(5), 2308–2322.
Erickson, B. A., Birnir, B., & Lavallée, D. (2011). Periodicity, chaos and localization in a Burridge–Knopoff model of an earthquake with rate-and-state friction. *Geophysical Journal International*, *187*(1), 178–198.
Erickson, B. A., & Dunham, E. M. (2014). An efficient numerical method for earthquake cycles in heterogeneous media: Alternating subbasin and surface-rupturing events on faults crossing a sedimentary basin. *Journal of Geophysical Research: Solid Earth*, *119*(4), 3290–3316.
Erickson, B. A., Jiang, J., Barall, M., Lapusta, N., Dunham, E. M., Harris, R., … others (2020). The community code verification exercise for simulating sequences of earthquakes and aseismic slip (SEAS). *Seismological Research Letters*, *91*(2A), 874–890.
Erickson, B. A., Jiang, J., Lambert, V., Barbot, S. D., Abdelmeguid, M., Almquist, M., … others (2023). Incorporating full elastodynamic effects and dipping fault geometries in community code verification exercises for simulations of earthquake sequences and aseismic slip (SEAS). *Bulletin of the Seismological Society of America*, *113*(2), 499–523.
Fang, Z., & Dunham, E. M. (2013). Additional shear resistance from fault roughness and stress levels on geometrically complex faults. *Journal of Geophysical Research: Solid Earth*, *118*(7), 3642–3654.
Fialko, Y., Sandwell, D., Agnew, D., Simons, M., Shearer, P., & Minster, B. (2002). Deformation on nearby faults induced by the 1999 Hector Mine earthquake. *Science*, *297*, 1858–1862.
Flores-Cuba, J., Oral, E., Idini, B., Liang, C., & Ampuero, J. P. (2024). Mechanisms and seismological signatures of rupture complexity induced by fault damage zones in fully-dynamic earthquake cycle models. *Geophysical Research Letters*, *51*(11), e2024GL108792.
Gabriel, A.-A., Ampuero, J.-P., Dalguer, L. A., & Mai, P. (2012). The transition of dynamic rupture styles in elastic media under velocity-weakening friction. *Journal of Geophysical Research: Solid Earth*, *117*(B9). Retrieved from `https://agupubs.onlinelibrary.wiley.com/doi/abs/10.1029/2012JB009468` doi: https://doi.org/10.1029/2012JB009468
Gabriel, A.-A., Garagash, D. I., Palgunadi, K. H., & Mai, P. (2024). Fault size–dependent fracture energy explains multiscale seismicity and cascading earthquakes. *Science*, *385*(6707), eadj9587.
Galvez, P., Somerville, P., Petukhin, A., Ampuero, J.-P., & Peter, D. (2020). Earthquake cycle modelling of multi-segmented faults: dynamic rupture and ground motion simulation of the 1992 M_w 7.3 Landers earthquake. *Pure and Applied Geophysics*, *177*, 2163–2179.
Gu, J.-C., Rice, J. R., Ruina, A., & Tse, S. T. (1984). Slip motion and stability of a single degree of freedom elastic system with rate and state dependent friction. *Journal of the Mechanics and Physics of Solids*, *32*(3), 167–196.
Hawthorne, J. C., & Rubin, A. M. (2013). Laterally propagating slow slip events in a rate and state friction model with a velocity-weakening to velocity-strengthening transition. *Journal of Geophysical Research: Solid Earth*, *118*(7), 3785–3808.
He, C., Wong, T.-f., & Beeler, N. (2003). Scaling of stress drop with recurrence interval and loading velocity for laboratory-derived fault strength relations. *Journal of Geophysical Research: Solid Earth*, *108*(B1).
He, C., Zhang, L., Liu, P., & Chen, Q.-F. (2023). Characterizing the final stage

of simulated earthquake nucleation governed by rate-and-state fault friction. *Journal of Geophysical Research: Solid Earth*, *128*(5), e2023JB026422.

Helmstetter, A., & Shaw, B. E. (2009). Afterslip and aftershocks in the rate-and-state friction law. *Journal of geophysical Research: Solid earth*, *114*(B1).

Herrendörfer, R., Van Dinther, Y., Gerya, T., & Dalguer, L. A. (2015). Earthquake supercycle in subduction zones controlled by the width of the seismogenic zone. *Nature Geoscience*, *8*(6), 471–474.

Hillers, G., Ben-Zion, Y., & Mai, P. (2006). Seismicity on a fault controlled by rate- and state-dependent friction with spatial variations of the critical slip distance. *Journal of Geophysical Research: Solid Earth*, *111*(B1).

Hillers, G., Mai, P., Ben-Zion, Y., & Ampuero, J.-P. (2007). Statistical properties of seismicity of fault zones at different evolutionary stages. *Geophysical Journal International*, *169*(2), 515–533.

Huang, L., Schwartz, S., & Brodsky, E. (2024). Microseismicity at the Time of a Large Creep Event on the Calaveras Fault is Unresponsive to Stress Changes. *Seismica*, *3*(2).

Huang, Y., & Ampuero, J.-P. (2011). Pulse-like ruptures induced by low-velocity fault zones. *Journal of Geophysical Research: Solid Earth*, *116*(B12).

Huang, Y., Ampuero, J.-P., & Helmberger, D. V. (2014). Earthquake ruptures modulated by waves in damaged fault zones. *Journal of Geophysical Research: Solid Earth*, *119*(4), 3133–3154.

Huang, Y., Meng, L., & Ampuero, J.-P. (2012). A dynamic model of the frequency-dependent rupture process of the 2011 Tohoku-Oki earthquake. *Earth, planets and space*, *64*, 1061–1066.

Idini, B., & Ampuero, J.-P. (2020). Fault-zone damage promotes pulse-like rupture and back-propagating fronts via quasi-static effects. *Geophysical Research Letters*, *47*(23), e2020GL090736.

Ito, R., & Kaneko, Y. (2023). Physical mechanism for a temporal decrease of the Gutenberg-Richter b-value prior to a large earthquake. *Journal of Geophysical Research: Solid Earth*, *128*(12), e2023JB027413.

Jiang, J., & Fialko, Y. (2016). Reconciling seismicity and geodetic locking depths on the anza section of the san jacinto fault. *Geophysical Research Letters*, *43*(20), 10–663.

Jiang, J., & Lapusta, N. (2016). Deeper penetration of large earthquakes on seismically quiescent faults. *Science*, *352*(6291), 1293–1297.

Jin, Z., & Fialko, Y. (2020). Finite slip models of the 2019 Ridgecrest earthquake sequence constrained by space geodetic data and aftershock locations. *Bulletin of the Seismological Society of America*, *110*(4), 1660–1679.

Kaneko, Y., Ampuero, J.-P., & Lapusta, N. (2011). Spectral-element simulations of long-term fault slip: Effect of low-rigidity layers on earthquake-cycle dynamics. *Journal of Geophysical Research: Solid Earth*, *116*(B10).

Kaneko, Y., Fialko, Y., Sandwell, D., Tong, X., & Furuya, M. (2013). Interseismic deformation and creep along the central section of the North Anatolian Fault (Turkey): InSAR observations and implications for rate-and-state friction properties. *Journal of Geophysical Research: Solid Earth*, *118*(1), 316–331.

Kaneko, Y., & Lapusta, N. (2010). Supershear transition due to a free surface in 3-D simulations of spontaneous dynamic rupture on vertical strike-slip faults. *Tectonophysics*, *493*(3-4), 272–284.

Kato, N., & Tullis, T. E. (2001). A composite rate-and state-dependent law for rock friction. *Geophysical research letters*, *28*(6), 1103–1106.

Kroll, K. A., Dieterich, J. H., Richards-Dinger, K. B., & Oglesby, D. D. (2023). 3-D Simulations of earthquakes rupture jumps: 1. Homogeneous pre-stress conditions. *Geophysical Journal International*, *234*(1), 395–403.

Lapusta, N., & Rice, J. R. (2003). Nucleation and early seismic propagation of small and large events in a crustal earthquake model. *Journal of Geophysical*

Research: Solid Earth, *108* (B4).
Lapusta, N., Rice, J. R., Ben-Zion, Y., & Zheng, G. (2000). Elastodynamic analysis for slow tectonic loading with spontaneous rupture episodes on faults with rate-and state-dependent friction. *Journal of Geophysical Research: Solid Earth*, *105* (B10), 23765–23789.
Lee, J.-J., & Bruhn, R. L. (1996). Structural anisotropy of normal fault surfaces. *Journal of Structural Geology*, *18* (8), 1043–1059.
Li, M., Niemeijer, A., & van Dinther, Y. (2025). Earthquake nucleation and slip behavior altered by stochastic normal stress heterogeneity. *Journal of Geophysical Research: Solid Earth*, *130* (1), e2024JB029857.
Li, V. C., & Rice, J. R. (1987). Crustal deformation in great California earthquake cycles. *Journal of Geophysical Research: Solid Earth*, *92*, 11533–11551.
Linde, A. T., Suyehiro, K., Miura, S., Sacks, I. S., & Takagi, A. (1988). Episodic aseismic earthquake precursors. *Nature*, *334* (6182), 513–515.
Lindsey, E. O., & Fialko, Y. (2016). Geodetic constraints on frictional properties and earthquake hazard in the Imperial Valley, Southern California. *Journal of Geophysical Research: Solid Earth*, *121* (2), 1097–1113.
Linker, M., & Dieterich, J. H. (1992). Effects of variable normal stress on rock friction: Observations and constitutive equations. *Journal of Geophysical Research: Solid Earth*, *97* (B4), 4923–4940.
Liu, D., Duan, B., & Luo, B. (2020). EQsimu: a 3-D finite element dynamic earthquake simulator for multicycle dynamics of geometrically complex faults governed by rate-and state-dependent friction. *Geophysical Journal International*, *220* (1), 598–609.
Liu, Y., & Rice, J. R. (2007). Spontaneous and triggered aseismic deformation transients in a subduction fault model. *Journal of Geophysical Research: Solid Earth*, *112* (B9).
Luo, Y., & Ampuero, J.-P. (2018). Stability of faults with heterogeneous friction properties and effective normal stress. *Tectonophysics*, *733*, 257–272.
Luo, Y., & Liu, Z. (2019). Slow-slip recurrent pattern changes: Perturbation responding and possible scenarios of precursor toward a megathrust earthquake. *Geochemistry, Geophysics, Geosystems*, *20* (2), 852–871.
Maurer, J. (2024). Statistical distribution of static stress resolved onto geometrically-rough faults. *Seismica*, *3* (2).
Melgar, D., Taymaz, T., Ganas, A., Crowell, B. W., Öcalan, T., Kahraman, M., ... others (2023). Sub-and super-shear ruptures during the 2023 Mw 7.8 and Mw 7.6 earthquake doublet in SE Türkiye.
Mitchell, E., Fialko, Y., & Brown, K. (2015). Frictional properties of gabbro at conditions corresponding to slow slip events in subduction zones. *Geochemistry, Geophysics, Geosystems*, *16* (11), 4006–4020.
Mitchell, E., Fialko, Y., & Brown, K. (2016). Velocity-weakening behavior of Westerly granite at temperature up to 600° C. *Journal of Geophysical Research: Solid Earth*, *121*, 6932–6946.
Molina-Ormazabal, D., Ampuero, J.-P., & Tassara, A. (2023). Diverse slip behaviour of velocity-weakening fault barriers. *Nature Geoscience*, *16* (12), 1200–1207.
Nadeau, R. M., & Johnson, L. R. (1998). Seismological studies at Parkfield VI: Moment release rates and estimates of source parameters for small repeating earthquakes. *Bulletin of the Seismological Society of America*, *88* (3), 790–814.
Nagata, K., Nakatani, M., & Yoshida, S. (2012). A revised rate-and state-dependent friction law obtained by constraining constitutive and evolution laws separately with laboratory data. *Journal of Geophysical Research: Solid Earth*, *117* (B2).
Nie, S., & Barbot, S. (2022). Rupture styles linked to recurrence patterns in seismic cycles with a compliant fault zone. *Earth and Planetary Science Letters*, *591*, 117593.
Niu, Z., Gabriel, A.-A., Seelinger, L., & Igel, H. (2024). Modeling and quantifying

parameter uncertainty of co-seismic non-classical nonlinearity in rocks. *Journal of Geophysical Research: Solid Earth*, *129*(1), e2023JB027149.

Oeser, J., Bunge, H.-P., & Mohr, M. (2006). Cluster design in the earth sciences tethys. In *International conference on high performance computing and communications* (pp. 31–40).

Ozawa, S., & Ando, R. (2021). Mainshock and aftershock sequence simulation in geometrically complex fault zones. *Journal of Geophysical Research: Solid Earth*, *126*(2), e2020JB020865.

Perez-Silva, A., Kaneko, Y., Savage, M., Wallace, L., Li, D., & Williams, C. (2022). Segmentation of Shallow Slow Slip Events at the Hikurangi Subduction Zone Explained by Along-Strike Changes in Fault Geometry and Plate Convergence Rates. *Journal of Geophysical Research: Solid Earth*, *127*(1), e2021JB022913.

Perfettini, H., & Ampuero, J.-P. (2008). Dynamics of a velocity strengthening fault region: Implications for slow earthquakes and postseismic slip. *Journal of Geophysical Research: Solid Earth*, *113*(B9).

Perfettini, H., & Avouac, J.-P. (2007). Modeling afterslip and aftershocks following the 1992 Landers earthquake. *Journal of Geophysical Research: Solid Earth*, *112*.

Perfettini, H., Schmittbuhl, J., & Cochard, A. (2003a). Shear and normal load perturbations on a two-dimensional continuous fault: 1. Static triggering. *Journal of Geophysical Research: Solid Earth*, *108*(B9).

Perfettini, H., Schmittbuhl, J., & Cochard, A. (2003b). Shear and normal load perturbations on a two-dimensional continuous fault: 2. Dynamic triggering. *Journal of Geophysical Research: Solid Earth*, *108*(B9).

Pignalberi, F., Giorgetti, C., Noël, C., Marone, C., Collettini, C., & Scuderi, M. M. (2024). The effect of normal stress oscillations on fault slip behavior near the stability transition from stable to unstable motion. *Journal of Geophysical Research: Solid Earth*, *129*(2), e2023JB027470.

Pranger, C. C. (2020). *Unstable physical processes operating on self-governing fault systems, improved modeling methodology* (Unpublished doctoral dissertation). ETH Zurich.

Ranjith, K., & Rice, J. R. (1999). Stability of quasi-static slip in a single degree of freedom elastic system with rate and state dependent friction. *Journal of the Mechanics and Physics of Solids*, *47*(6), 1207–1218.

Renard, F., & Candela, T. (2017). Scaling of fault roughness and implications for earthquake mechanics. *Fault zone dynamic processes: Evolution of fault properties during seismic rupture*, 195–215.

Renard, F., Voisin, C., Marsan, D., & Schmittbuhl, J. (2006). High resolution 3D laser scanner measurements of a strike-slip fault quantify its morphological anisotropy at all scales. *Geophysical Research Letters*, *33*(4).

Rice, J. R. (1993). Spatio-temporal complexity of slip on a fault. *Journal of Geophysical Research: Solid Earth*, *98*(B6), 9885–9907.

Rice, J. R., & Ben-Zion, Y. (1996). Slip complexity in earthquake fault models. *Proceedings of the National Academy of Sciences*, *93*(9), 3811–3818.

Romanet, P., Sato, D. S., & Ando, R. (2020). Curvature, a mechanical link between the geometrical complexities of a fault: Application to bends, kinks and rough faults. *Geophysical Journal International*, *223*(1), 211–232.

Ross, Z. E., Cochran, E. S., Trugman, D. T., & Smith, J. D. (2020). 3D fault architecture controls the dynamism of earthquake swarms. *Science*, *368*(6497), 1357–1361.

Rousset, B., Bürgmann, R., & Campillo, M. (2019). Slow slip events in the roots of the San Andreas fault. *Science advances*, *5*(2), eaav3274.

Rubin, A. M. (2008). Episodic slow slip events and rate-and-state friction. *Journal of Geophysical Research: Solid Earth*, *113*(B11).

Rubin, A. M., & Ampuero, J.-P. (2005). Earthquake nucleation on (aging) rate and state faults. *Journal of Geophysical Research: Solid Earth*, *110*(B11).

Ruina, A. (1983). Slip instability and state variable friction laws. *Journal of Geophysical Research: Solid Earth*, *88*(B12), 10359–10370.

Schliwa, N., Gabriel, A.-A., Premus, J., & Gallovič, F. (2024). The linked complexity of coseismic and postseismic faulting revealed by seismo-geodetic dynamic inversion of the 2004 Parkfield earthquake. *Journal of Geophysical Research: Solid Earth*, *129*(12), e2024JB029410.

Schmedes, J., Archuleta, R. J., & Lavallée, D. (2010). Correlation of earthquake source parameters inferred from dynamic rupture simulations. *Journal of Geophysical Research: Solid Earth*, *115*(B3).

Shaw, B. E., & Rice, J. R. (2000). Existence of continuum complexity in the elastodynamics of repeated fault ruptures. *Journal of Geophysical Research: Solid Earth*, *105*(B10), 23791–23810.

Shi, Z., & Day, S. M. (2013). Rupture dynamics and ground motion from 3-D rough-fault simulations. *Journal of Geophysical Research: Solid Earth*, *118*(3), 1122–1141.

Song, J. Y., & McLaskey, G. C. (2024). Laboratory Experiments with Eleven Velocity-Weakening Patches Separated by Velocity-Strengthening Barriers Illuminate the Mechanisms Behind Apparent Inverse Fault Healing and Rapid Tremor Reversals. *AGU24*.

Tal, Y., & Gabrieli, T. (2024). Dual effect of roughness during earthquake rupture sequences on faults with strongly rate-weakening friction. *Earth and Planetary Science Letters*, *637*, 118738.

Taufiqurrahman, T., Gabriel, A.-A., Li, D., Ulrich, T., Li, B., Carena, S., … Gallovič, F. (2023). Dynamics, interactions and delays of the 2019 Ridgecrest rupture sequence. *Nature*, *618*(7964), 308–315.

Thakur, P., & Huang, Y. (2021). Influence of fault zone maturity on fully dynamic earthquake cycles. *Geophysical Research Letters*, *48*(17), e2021GL094679.

Thakur, P., Huang, Y., & Kaneko, Y. (2020). Effects of low-velocity fault damage zones on long-term earthquake behaviors on mature strike-slip faults. *Journal of Geophysical Research: Solid Earth*, *125*(8), e2020JB019587.

Thomas, M. Y., Lapusta, N., Noda, H., & Avouac, J.-P. (2014). Quasi-dynamic versus fully dynamic simulations of earthquakes and aseismic slip with and without enhanced coseismic weakening. *Journal of Geophysical Research: Solid Earth*, *119*(3), 1986–2004.

Thurber, C. H. (1996). Creep events preceding small to moderate earthquakes on the San Andreas fault. *Nature*, *380*(6573), 425–428.

Thurber, C. H., & Sessions, R. (1998). Assessment of creep events as potential earthquake precursors: application to the creeping section of the San Andreas fault, California. *pure and applied geophysics*, *152*, 685–705.

Tse, S. T., & Rice, J. R. (1986). Crustal earthquake instability in relation to the depth variation of frictional slip properties. *Journal of Geophysical Research: Solid Earth*, *91*(B9), 9452–9472.

Turner, A., Hawthorne, J. C., & Cattania, C. (2024). Partial ruptures cannot explain the long recurrence intervals of repeating earthquakes. *Journal of Geophysical Research: Solid Earth*, *129*(1), e2023JB027870.

Uchida, N., & Bürgmann, R. (2019). Repeating earthquakes. *Annual Review of Earth and Planetary Sciences*, *47*(1), 305–332.

Uphoff, C., May, D. A., & Gabriel, A.-A. (2023). A discontinuous Galerkin method for sequences of earthquakes and aseismic slip on multiple faults using unstructured curvilinear grids. *Geophysical Journal International*, *233*(1), 586–626.

Vavra, E. J., Fialko, Y., Rockwell, T., Bilham, R., Štěpančíková, P., Stemberk, J., … Stemberk, J. (2024). Characteristic slow-slip events on the Superstition Hills Fault, Southern California. , *51*(12), e2023GL107244.

Vyas, J. C., Gabriel, A.-A., Ulrich, T., Mai, P., & Ampuero, J.-P. (2023). How does thermal pressurization of pore fluids affect 3D strike-slip earthquake dynamics and ground motions? *Bulletin of the Seismological Society of America*, *113*(5), 1992–2008.

Waldhauser, F., & Schaff, D. P. (2008). Large-scale relocation of two decades of Northern California seismicity using cross-correlation and double-difference methods. *Journal of Geophysical Research: Solid Earth*, *113*(B8).

Wang, K., & Fialko, Y. (2014). Space geodetic observations and models of postseismic deformation due to the 2005 M7.6 Kashmir (Pakistan) earthquake. *Journal of Geophysical Research: Solid Earth*, *119*(9), 7306–7318.

Wang, S. (2024). Toward quantitative characterization of simulated earthquake-cycle complexities. *Scientific Reports*, *14*(1), 16811.

Wei, M., Kaneko, Y., Shi, P., & Liu, Y. (2018). Numerical modeling of dynamically triggered shallow slow slip events in New Zealand by the 2016 M_w 7.8 Kaikoura earthquake. *Geophysical Research Letters*, *45*(10), 4764–4772.

Wei, M., Sandwell, D., & Fialko, Y. (2009). A silent M4.8 slip event of October 3-6, 2006, on the Superstition Hills fault, Southern California. *Journal of Geophysical Research: Solid Earth*, B07402.

Yin, Y., Galvez, P., Heimisson, E. R., & Wiemer, S. (2023). The role of three-dimensional fault interactions in creating complex seismic sequences. *Earth and Planetary Science Letters*, *606*, 118056.

Yingdi, L., & Ampuero, J. P. (2017). Preprint: Tremor migration patterns and the collective behavior of deep asperities mediated by creep.

Yoshida, S., Maeda, T., & Kato, N. (2020). Earthquake triggering model based on normal-stress-dependent Nagata law: application to the 2016 Mie offshore earthquake. *Earth, Planets and Space*, *72*, 1–13.

Zhang, C., Oglesby, D. D., & Xu, G. (2006). Earthquake nucleation on dip-slip faults with depth-dependent frictional properties. *Journal of Geophysical Research: Solid Earth*, *111*(B7).

Zhao, B., Bürgmann, R., Wang, D., Zhang, J., Yu, J., & Li, Q. (2022). Aseismic slip and recent ruptures of persistent asperities along the alaska-aleutian subduction zone. *Nature Communications*, *13*(1), 3098.

Zhao, C., Mia, M. S., Elbanna, A., & Ben-Zion, Y. (2024). Dynamic rupture modeling in a complex fault zone with distributed and localized damage. *Mechanics of Materials*, *198*, 105139.

Ziv, A., & Cochard, A. (2006). Quasi-dynamic modeling of seismicity on a fault with depth-variable rate-and state-dependent friction. *Journal of Geophysical Research: Solid Earth*, *111*(B8).

Supporting Information for "Effects of Stress and Friction Heterogeneity on Spatiotemporal Complexity of Seismic and Aseismic Slip on Strike-Slip Faults"

Jeena Yun[1], Alice-Agnes Gabriel[1,2], Dave A. May[1], and Yuri Fialko[1]

[1]Scripps Institution of Oceanography, University of California San Diego, La Jolla, CA, USA

[2]Department of Earth and Environmental Sciences, Ludwig-Maximilians Universität München, Munich, Germany

Contents of this file

Text S1. Numerical Resolution of Volumetric Discontinuous Galerkin Seismic Cycle Models with *Tandem*

We analyze the two most important length scales that need to be resolved in seismic cycle models: the process zone size (Λ_0) and the critical nucleation size (L_∞ defined in the main text; Erickson et al., 2020; Jiang et al., 2022; Rice, 1993). The quasi-static process zone is the area near the rupture front where the fault dynamically weakens, which can be estimated as follows (Day et al., 2005):

$$\Lambda_0 = C\frac{\mu D_{RS}}{b\sigma_n}$$

with C being a constant of an order of 1. The most complex aging law model (A2 model in the main text; see Section 3.3) has the smallest values for Λ_0 and L_∞ are 25.47 m and 39.83 m, respectively.

Tandem is a volume-based discontinuous Galerkin code (Uphoff et al., 2023) and must discretize the 2D domain with sufficiently small elements to resolve both Λ_0 and L_∞. To ease computation, we use static gradual mesh coarsening, in which high resolution can be localized in a region around the fault. The minimum element size is prescribed at the fault.

The high-order basis function in *Tandem*'s discontinuous Galerkin scheme provides sub-element resolution, allowing larger element sizes compared to low-order methods without sacrificing accuracy (Uphoff et al., 2023). In this study, we use a basis function of polynomial degree 6 and take an on-fault (minimum) element size (Δz) of 25 m, resulting in an effective element size of $\sim$ 4 m per degree of freedom. This model resolves the minimum length scale with 6 elements. The element sizes gradually increase up to 50 km at boundaries, located 400 km away from the fault.

To verify the effective resolution of the model, we compare this model with a higher resolution model using a smaller Δz of 10 m, resulting in the smallest effective element size of $\sim$ 1.6 m. The two models evolve identically until $\sim$ 150 years of simulation time. Afterward, minor deviations gradually accumulate (Fig. S4). These deviations are likely resulting from accumulated round-off errors over time. Since the problem is highly nonlinear, small round-off errors can lead to a visible deviation between equivalent models (i.e., Erickson et al., 2020). To reach 300 years of simulation time, the $\Delta z = 10$ m model takes 3 times more steps than the $\Delta z = 25$ m model, which potentially allows more round-off error to accrue.

Regardless of the minor difference between the two models, the characteristic complexities in the earthquake cycle (e.g., the cascade of partial ruptures, shallow and deep slow slip events, and a range of hypocenter depths) spontaneously emerge in both models. The qualitative similarity implies that these complexities are not the artifacts observed in inherently discrete models induced by the oversized cells (Erickson et al., 2020; Rice, 1993; Rice & Ben-Zion, 1996).

For slip law simulations, finer spatial resolution is required to properly resolve the nucleation size (Ampuero & Rubin, 2008). Ampuero and Rubin (2008) used a grid spacing of $L_b/50 - L_b/150$ in their simulations with the slip law, where $L_b = \mu D_{RS}/b\sigma_n$ (Dieterich, 1992). The slip law reference model ($\overline{D_{RS}} = 10$ m; see Section 3.2 in the main text) has minimum $L_b = 127$ m and we use $\Delta z = L_b/10 \approx 10$ m, resolving L_b with 76 elements. The A10 model (see Section 3.2 in the main text) uses Δz of 125 m, which is a factor of 5 larger than the aging law reference model, reflecting the difference in $\overline{D_{RS}}$.

References

Ampuero, J.-P., & Rubin, A. M. (2008). Earthquake nucleation on rate and state faults – Aging and slip laws. *Journal of Geophysical Research: Solid Earth*, *113*(B1).

Day, S. M., Dalguer, L. A., Lapusta, N., & Liu, Y. (2005). Comparison of finite difference and boundary integral solutions to three-dimensional spontaneous rupture. *Journal of Geophysical Research: Solid Earth*, *110*(B12).

Dieterich, J. H. (1992). Earthquake nucleation on faults with rate-and state-dependent strength. *Tectonophysics*, *211*(1-4), 115–134.

Erickson, B. A., Jiang, J., Barall, M., Lapusta, N., Dunham, E. M., Harris, R., ... others (2020). The community code verification exercise for simulating sequences of earthquakes and aseismic slip (SEAS). *Seismological Research Letters*, *91*(2A), 874–890.

Jiang, J., Erickson, B. A., Lambert, V. R., Ampuero, J.-P., Ando, R., Barbot, S., ... others (2022). Community-driven code comparisons for three-dimensional dynamic modeling of sequences of earthquakes and aseismic slip. *Journal of Geophysical Research: Solid Earth*, *127*(3), e2021JB023519.

Rice, J. R. (1993). Spatio-temporal complexity of slip on a fault. *Journal of Geophysical Research: Solid Earth*, *98*(B6), 9885–9907.

Rice, J. R., & Ben-Zion, Y. (1996). Slip complexity in earthquake fault models. *Proceedings of the National Academy of Sciences*, *93*(9), 3811–3818.

Uphoff, C., May, D. A., & Gabriel, A.-A. (2023). A discontinuous Galerkin method for sequences of earthquakes and aseismic slip on multiple faults using unstructured curvilinear grids. *Geophysical Journal International*, *233*(1), 586–626.

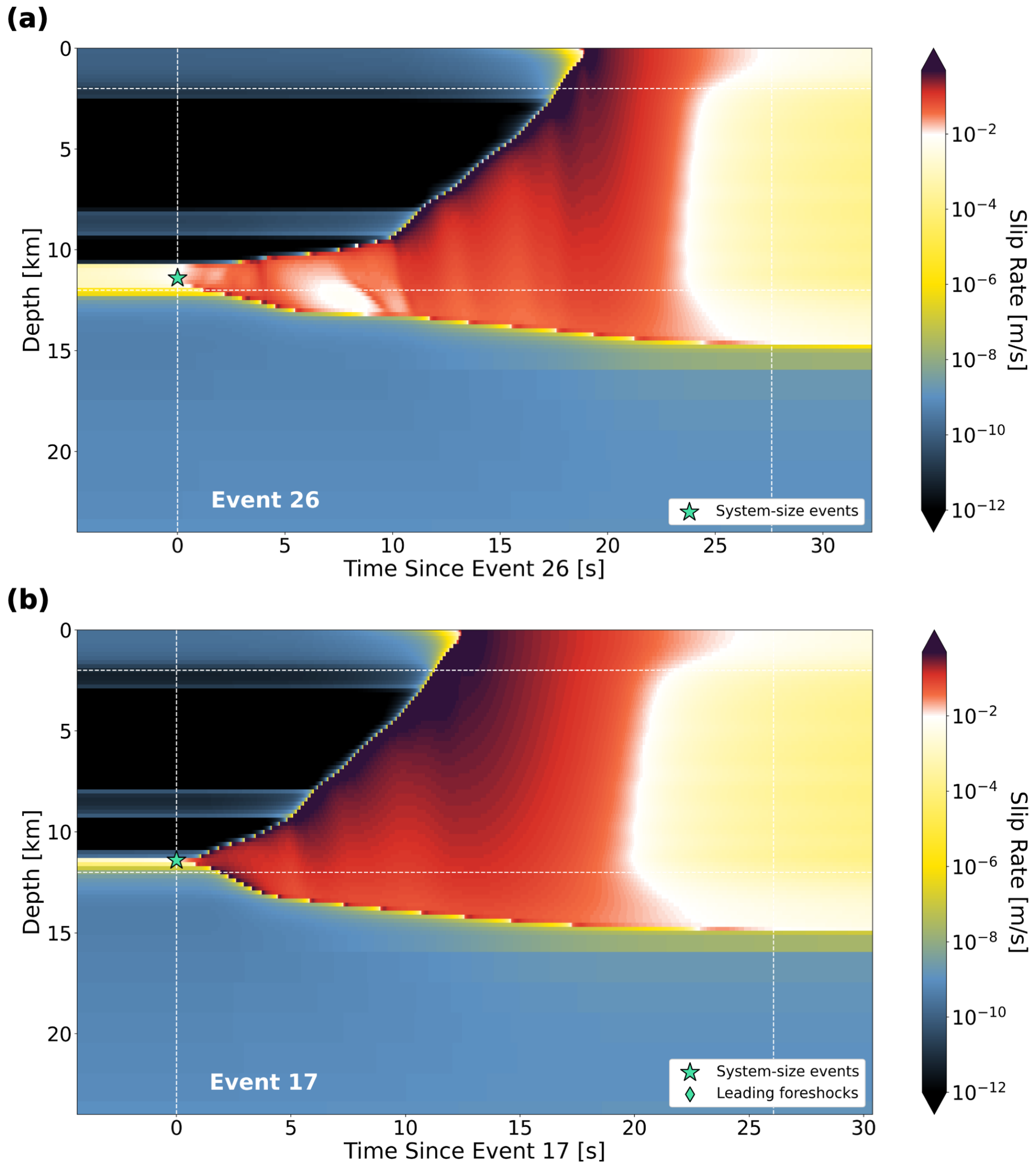

Figure S1. Spatiotemporal evolution of slip rate during one of the system-size earthquakes in seismic cycle models (a) with and (b) without a low-rigidity fault zone (see Section 3.2 in the main text). (a) Zoom-in of event 26 in the model with a low-rigidity fault zone (NDFZ model), shown in Figure 4a in the main text. Multiple slip pulses with some back-propagating rupture fronts are observed. (b) Zoom-in of event 17 in the model with low-rigidity bulk model but without a low-rigidity fault zone (ND model), shown in Figure 4b in the main text. Green stars indicate the hypocenter locations of system-size earthquakes.

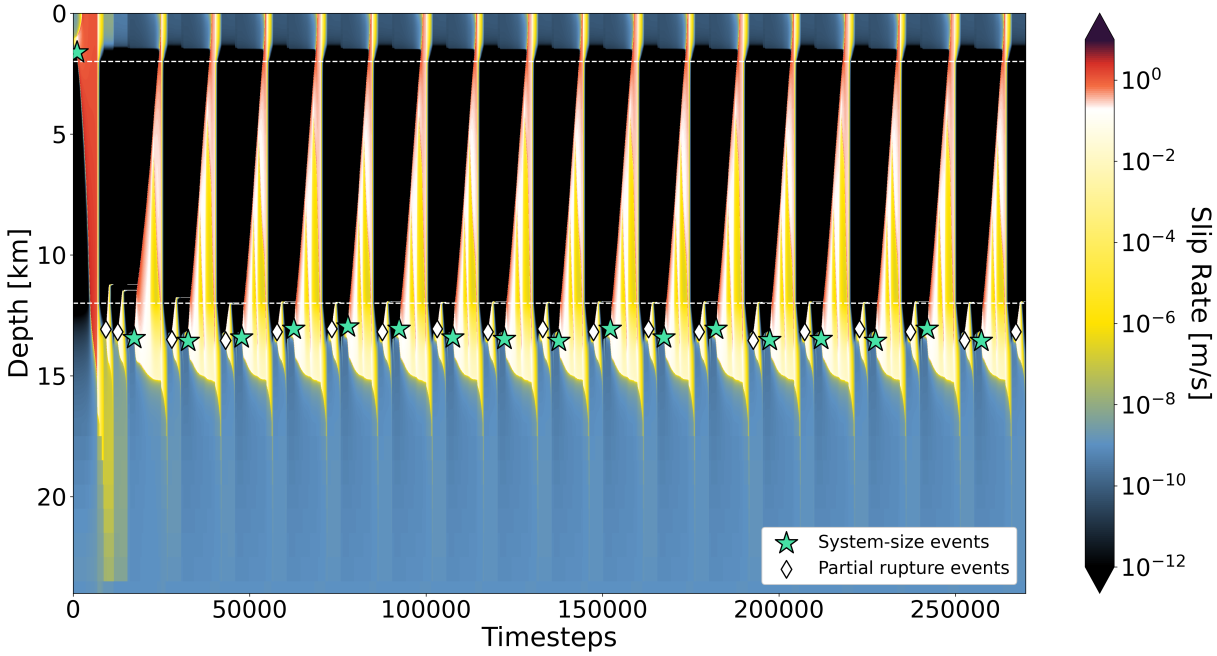

Figure S2. Spatiotemporal evolution of slip rate of a homogeneous model with a uniform $W/L_\infty = 251$ at all depths, same as the highest W/L_∞ value of the most complex aging law seismic cycle model (A2 model in the main text). Green stars and white diamonds indicate the hypocenter locations of system-size earthquakes and partial rupture events, respectively.

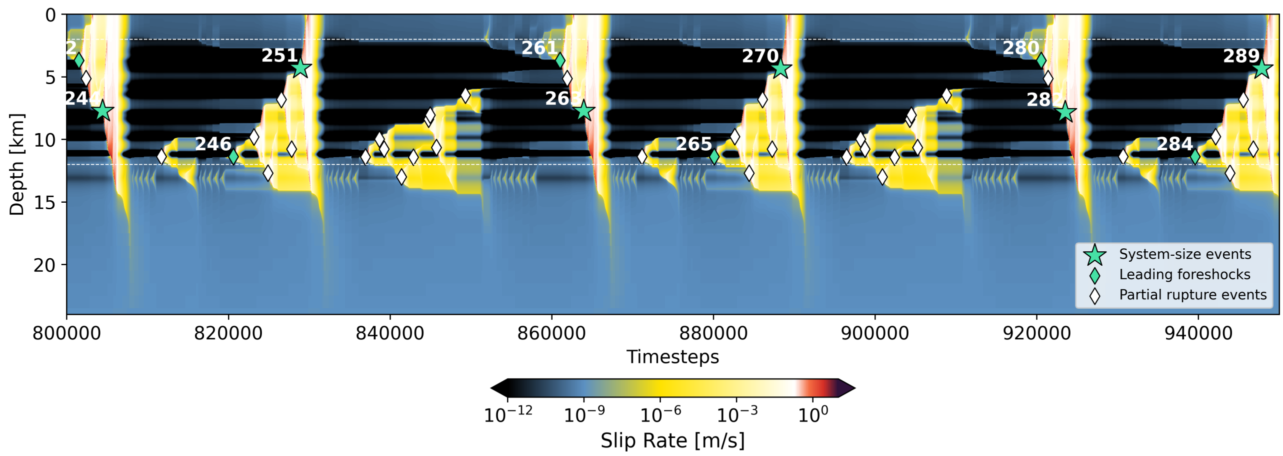

Figure S3. Same as Figure 5a in the main text, but plotted between 2,317 yr and 2,681 yr of simulation time, after the transition into the cycle-invariant regime.

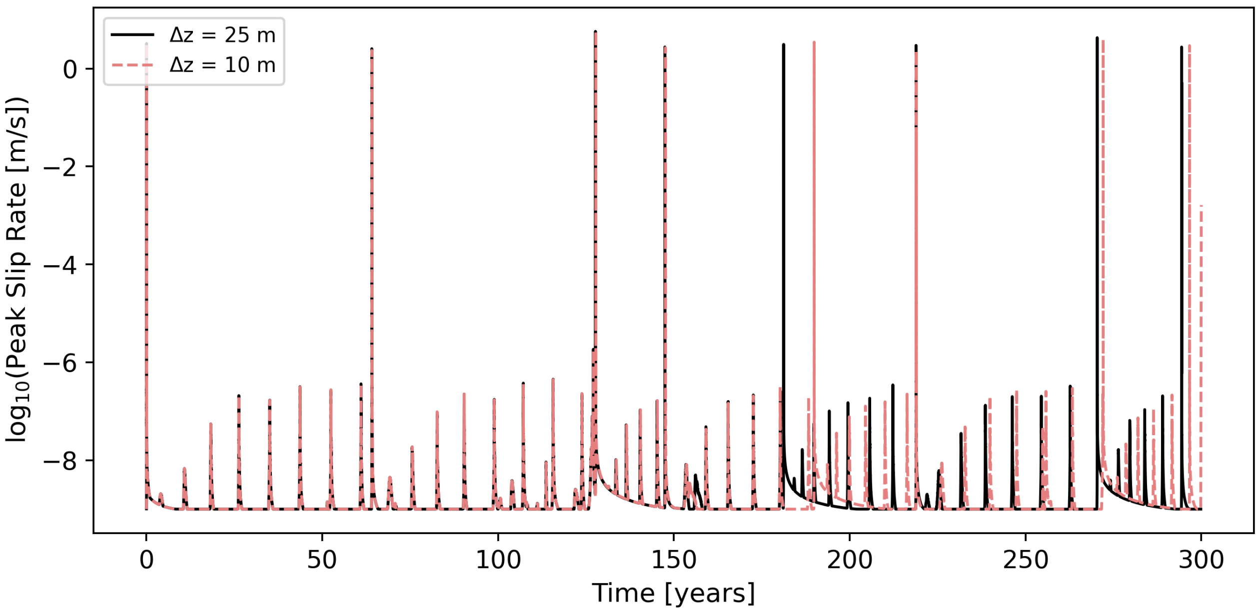

Figure S4. Peak slip rate evolution of the most complex aging law seismic cycle model (A2 model in the main text) using $\Delta z = 25$ m (black solid line) and $\Delta z = 10$ m (pink dashed line). The two models agree well before ~ 150 years.